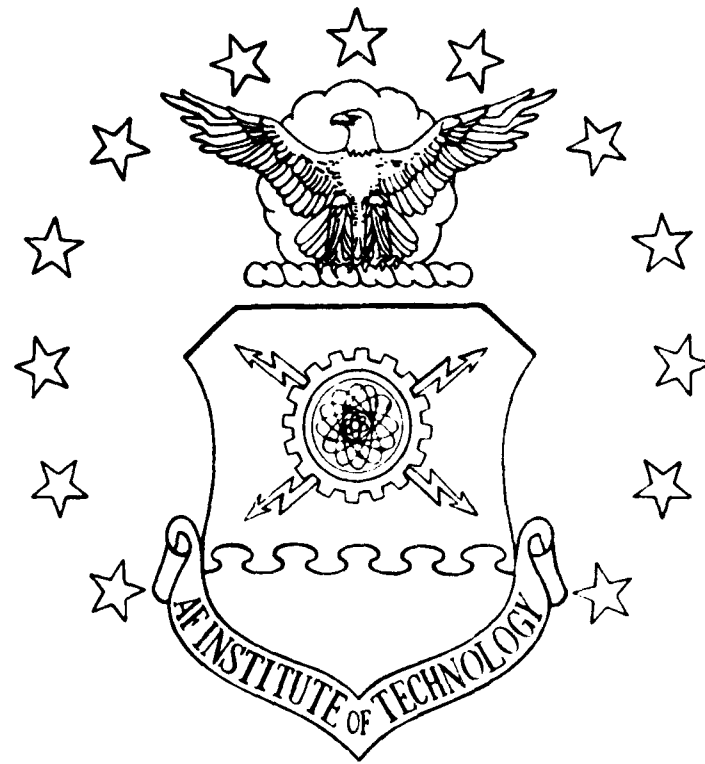DETERMINATION OF LATERAL SPREAD

OF NUCLEAR FALLOUT PATTERNS

THESIS

David P. Schneider
Captain, USA
PH
AFIT/GNE/ENP/86M-12

DTIC
ELECTE
OCT 16 1986
B

DEPARTMENT OF THE AIR FORCE

AIR UNIVERSITY

AIR FORCE INSTITUTE OF TECHNOLOGY

Wright-Patterson Air Force Base, Ohio

DETERMINATION OF LATERAL SPREAD

OF NUCLEAR FALLOUT PATTERNS

THESIS

David P. Schneider
Captain, USA

AFIT/GNE/~ENP~ *PH*/86M-12

DTIC
ELECTE
OCT 16 1986

B

DETERMINATION OF LATERAL SPREAD OF NUCLEAR FALLOUT PATTERNS

THESIS

Presented to the Faculty of the School of Engineering

of the Air Force Institute of Technology

Air University

In Partial Fulfillment of the

Requirements for the Degree of

Master of Science in Nuclear Engineering

David P. Schneider, B.S.

Captain, USA

March 1986

Preface

The purpose of this study is to determine how wind shear affects the lateral spread of fallout patterns. Several mathematical expressions are currently in use to predict this growth. Determining which one is the most accurate is the focus and goal of this study. It may even be that none of these are correct. In that case, a new expression will be sought and, if possible, validated.

Fallout patterns clearly extend in both the downwind and crosswind directions. In the crosswind direction, perpendicular to the downwind direction, the fallout is usually considered to be distributed in a gaussian, or near-gaussian, manner. This gaussian distribution can be described by its characteristic width, σ . Thus, σ is a good predictor of the total lateral distribution of the fallout pattern. The models used throughout this study are oriented on determining this characteristic σ .

Many people on the staff and faculty of the Air Force Institute of Technology were very helpful to me during the course of this research. For their assistance, I am very grateful. I would most like to thank Dr. C. J. Bridgman for his continued support and patient tutelage from beginning to end.

Lastly, I would like to dedicate this effort to every soldier who has worn MOPP IV, much to his or her own discomfort, longer than necessary in order to avoid contamination, whether real or imagined.

David P. Schneider

Table of Contents

QUALITY
INSPECTED
1

PER CALL JC

A-1

List of Figures

List of Tables

Abstract

This study refines the method of determining the lateral spread of fallout from nuclear explosions. Lateral growth of a fallout "pattern" under the influence of torroidal growth, wind shear, and diffusive growth is examined to determine how best to calculate the extent of a fallout pattern as it grows with time.

Two models of the initial stabilized nuclear cloud are investigated to determine how best to model the initial conditions which define the starting positions of the fallout particles. A hybrid model, incorporating portions of both, is developed. The grounded locations of the fallout are calculated after examining the influence of horizontal winds on their trajectories. From this examination, with the assistance of a new mathematical derivation of σ_s, an improved formula for the prediction of lateral spread of fallout is tested and confirmed.

Certain fairly common assumptions about the atmosphere and the use of the DELFIC 100 equal-activity groups allow simplification of the treatment of the geophysical properties to the extent that the problem can be analyzed on a microcomputer using BASIC. Accuracy is not sacrificed for simplicity, yet the methods used can provide quicker, more accurate results than the large codes run on mainframe computers.

Although only a one megaton explosion is examined in detail, the methods are applicable to the full range of strategic nuclear weapons.

DETERMINATION OF LATERAL SPREAD

OF NUCLEAR FALLOUT PATTERNS

I. Introduction

More than ever before, accurate and timely information
has become the cornerstone of sound tactical and strategic
decisions by military leaders. In this age of sophisticated
nuclear weapons and near "real-time" intelligence, brought about
by micro-miniaturization and advanced electronics, it is
surprising to find that little has been done to provide planners
with methods of determining nuclear weapons effects that are
also advanced, quick, and relatively easy to use. In fact, much
of today's planning is based on research that was stopped in the
1960's. Although atmospheric testing of nuclear weapons was
stopped as a result of the Nuclear Test Ban Treaty, there remain
areas of ambiguity and uncertainty in the analysis of the data
obtained during those tests.

Advances in peripheral areas, such as atmospherics, can
be applied to the original data from atmospheric tests to pro-
vide greater understanding of the processes involved. Increased
understanding could lead to improvements in accuracy and speed.

1

Although some nuclear effects may never be fully understood, others can already be more fully explained with the current state of knowledge.

Hopefully, this study will further understanding in one area of nuclear weapon effects. That area is, specifically, the growth of the lateral spread of the fallout pattern with respect to time due to crosswind shear. From an analysis of the forces which create nuclear clouds, the transportation of those clouds through the atmosphere, and the resulting pattern of fallout created on the ground, an expression relating the time of arrival of the fallout and the characteristic width of the fallout pattern (defined as "sigma", σ , from the standard definition of a Gaussian distribution) can be developed for a variety of initial conditions. The expressions developed in this manner will be compared against the optimum "full-physics" model of fallout pattern formation to determine which expression most closely replicates the actual process.

II. Problem Statement

There are currently two primary equations which compete for use in determining the lateral growth of fallout patterns. These equations, which are explained in the next chapter, are both empirical or semi-empirical and are the result of different methods of analysis, yet they are supposed to predict the same degree of lateral growth in a particular situation when they are used. This research effort focuses on determining which of these equations more accurately predicts the lateral growth. There exists the possibility that neither one of them predicts the fallout pattern as well as a new and different equation which is presented here.

In short, the purpose of this research is to determine what equation best predicts the lateral growth of a fallout pattern with respect to time.

III. Background

Unique Terms

Fallout prediction uses some terms that can be confusing when their specific definition within the field is not made clear. As a starting point, five definitions are included here.

Downwind. It is convenient to use a standard cartesian coordinate system as an initial reference frame. As can be seen in Figure 1, the X axis is co-labeled as the "Downwind" axis. Because the process of fallout formation occurs in the atmosphere, it is critical to define the orientation of this coordinate system with respect to that same atmosphere. For the purposes of this research, the following convention is chosen for determining the orientation of the downwind axis. The wind direction at the altitude of the center of the stabilized nuclear cloud (this term will be further defined in Chapter V) is identical to the direction of the X axis. The downwind direction is, then, the direction in which a nuclear cloud would drift if the wind were blowing from the same direction at all altitudes.

Crosswind. Just as the Y axis is translated ninety degrees from the X axis in a cartesian coordinate system, the Crosswind axis represents an axis that has been rotated ninety degrees from the downwind axis. Using this definition, the crosswind term refers to any component of the wind or any other force which acts perpendicular to the downwind axis. (See Figure 1)

4

Shear. "Shear" is defined as the magnitude of the change in both speed and direction between any two wind vectors. Naturally, all wind vectors occuring in the atmosphere will have three components corresponding to the three axes of the reference frame. The specific formulation of the shear forces as they pertain to this study are further defined in Chapter VI.

Sigma. The standard definition of a gaussian, or Normal probability function (1:927) is,

$$P(x) = \frac{1}{\sqrt{2\pi}\sigma} e^{-1/2[(x-\mu)/\sigma]^2}$$

where the probability of an occurrence, $P(x)$, is defined as a function of the mean, μ, and the standard deviation, σ. "Sigma", or σ, is alternatively defined as the standard deviation, the dispersion, or even as the characteristic width of the distribution. The fallout pattern on the ground will be modeled with the gaussian distribution in the crosswind direction. Why this is the case will be shown later. Therefore, σ_y is the characteristic width of the fallout pattern in the crosswind direction.

Disktosser. A "Disktosser" is the common term for a type of numerical fallout code which uses a discrete mesh of mono-sized particle disks to model the nuclear cloud. The disktosser "tosses" each of the disks that characterize the initial cloud into a given wind field and computes a grounded location for each disk based on the wind field and the parameters of the

5

atmosphere. The grounded locations of all the disks are then combined to form fallout patterns.
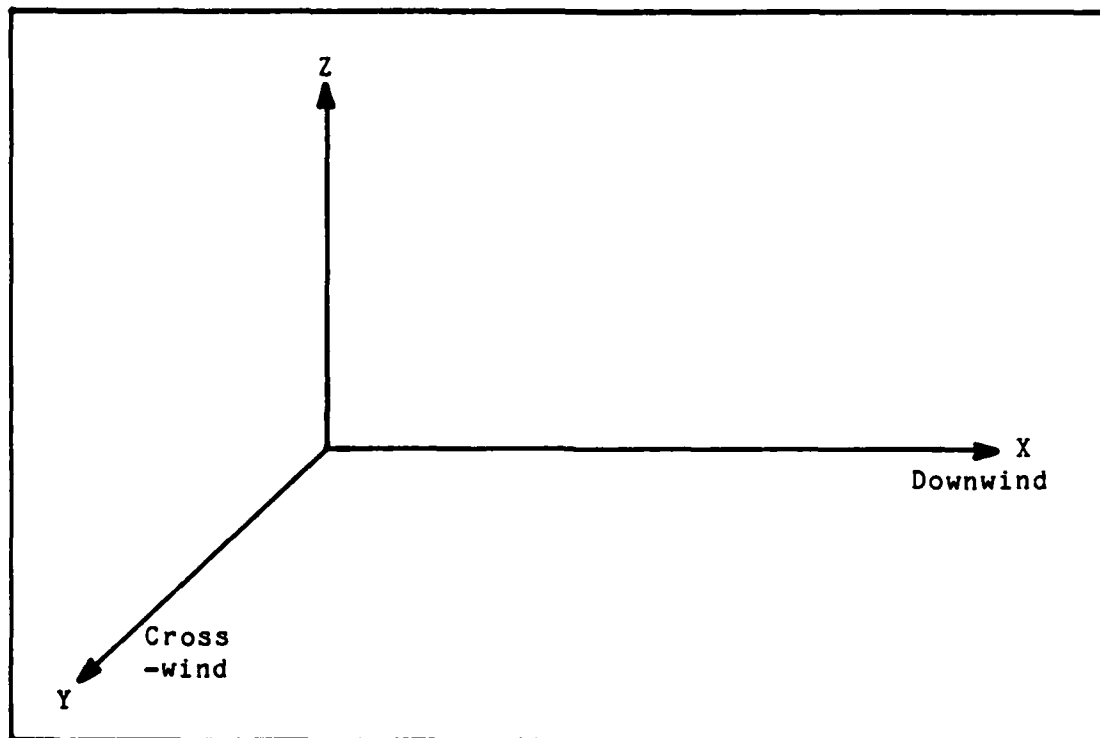
Figure 1. The Reference Frame

Method of Attack

Two methods might be used to determine which empirical equation is best. The first method would have been to run the data from a variety of atmospheric tests through one of the available fallout codes. All of the parameters would be held constant. Only the line of code that would predict the growth of the width of the pattern due solely to the crosswind shear would change. In theory, whichever version of the crosswind shear formula produced the most accurate fallout pattern (compared to those measured at test time) would then have been the best.

6

Unfortunately, there were simply too many external variables which were not recorded during the various tests. An example of the difficulty of such an approach might best be illustrated by a quotation from The Effects of Nuclear Weapons by S. Glasstone and P.J. Dolan where they explain a fallout pattern from a megaton-size explosion.

> "However, other patterns are possible; one, for example, ascribes the large radiation doses on the northern islands of Rongelap Atoll to a hot spot and brings the 3000-rad contour line in much closer to Bikini Atoll. Because of the absence of observations from large areas of ocean, the choice of the fallout pattern is largely a matter of guesswork. (2:436)

For the most part, nuclear tests conducted over land, although not in the megaton range, are also a product of the same kind of analysis. In short, there are too many variables to conduct a thorough a posteriori analysis of past weapons tests at the moment.

The second method, which relies less on published data and more on the physics of the actual process of transporting the particles through the atmosphere, becomes the method of choice after reviewing the available published data on atmospheric shots. This method involves modeling the individual phenomena as closely as possible with computer models. Each model is designed to duplicate, as closely as possible, the actual processes. (Such codes might be called "full-physics" codes.) These might be divided into three main phases of fallout pattern formation. These three phases are 1) cloud formation, 2)

7

particle fall, and 3) particle accumulation on the ground.
Combining all three phases produces the location, on the ground,
of a particular crosswind portion of the complete grounded
pattern. Adding all these portions, or slices, results in a
pattern that can be analyzed to determine how the pattern grew
with time. Then, the pattern of growth predicted by the model
will be compared with the two expressions to be shown next.

The major disadvantage of the modeling method is that it
does not lend itself to comparison with an actual explosion.
However, its ability for rigid comparison between the parameters
and analysis of the physics involved allow for more precise
isolation of the wind shear term. This is a clear advantage.

The Two Primary Equations

WSEG-10. One of the pioneering efforts to quantify and
simplify what was then known about nuclear fallout is WSEG
Research Memorandum No.10 - An Analytic Model of Close-In
Deposition of Fallout for Use in Operational-Type Studies. This
report, written in 1959, has been modified several times in the
intervening years in an attempt to more closely match the
experimental data obtained from the atmospheric tests (3:3-4).
However, the method of calculating the lateral growth of the
fallout pattern has not been significantly modified from the
original method as shown in WSEG-10. The only modification to
the original formulation is a refinement of the low-yield (in
the kiloton range) deposition rate. This refinement produces an

8

enhanced fallout pattern in the vicinity of ground zero for early times. The change is achieved by refining the input parameters (4:2-3), though, not by altering the basic method of calculation. Therefore, the underlying formulation of σ as used by WSEG-10 can be extracted from their original equation which defines the total crosswind spread. The total crosswind spread is caused by three main contributors, which, depending on the time at which the fallout pattern is analyzed, have different degrees of effect. The three contributors are cloud rise spreading, torroidal spreading after cloud stabilization, and crosswind shear effects. The complete formulation of crosswind spread (5:14) is,

$$\sigma_y{}^2 = \sigma_0{}^2 + [(8x\sigma_0{}^2)/L] + [S_y\sigma_h(x/W)]^2 \qquad (km) \qquad (1)$$

where

σ_y is the total crosswind spread (km)

σ_0 is the width of the initial stabilized cloud center (km)

x is the downwind distance at which the spread is desired

L is an empirical constant determined by yield

S_y is the effective shear (km/km-hr)

σ_h is the width of the vertical distribution of the stabilized cloud (km)

W is the effective wind speed in the downwind direction.

Since $x = Wt_a$ where t_a is the arrival time, the WSEG form may be written as,

9

$$\sigma_y{}^2 = \sigma_0{}^2 + 8t_a\sigma_0{}^2/T_c + (S_y t_a \sigma_h)^2 \quad \text{(km)} \quad \text{(1a)}$$

where $T_c = L/W$ is also empirical and the other variables are defined above.

With the aid of an assumption, equation (1) can be reduced as follows. The second term, $(8x\sigma_0{}^2/L)$, representsthe growth due to torroidal circulation. As a result, of observations of actual clouds, WSEG suggests that this growth continues for the first three hours of cloud formation and, thereafter, ceases to be significant. Thus for t_a greater than 3 hours the second term also becomes a constant. And,

$$\sigma_y{}^2(t) = \sigma_0{}^2 + 4\sigma_0{}^2/T_c + (S_y\sigma_h t_a)^2 = (\sigma_3{}^*)^2 + (S_y\sigma_h t_a)^2 \quad \text{(km)} \quad \text{(2)}$$

where $\sigma_3{}^*$ is the cloud width at 3 hours less the shear growth effects.

Without derivation, WSEG (Weapon Systems Evaluation Group) determined that the shear contribution to lateral growth was the final term $(S_y\sigma_h t_a)$. Designating this term by σ_s, and solving for σ_s produces an equation that defines the spreading due to shear according to WSEG as,

$$\sigma_s = \sqrt{\sigma_y{}^2 - \sigma_3{}^{*2}} \quad \text{(km)} \quad \text{(3)}$$

The authors do not include a derivation of equation (1) anywhere in WSEG-10 (5:11). However, its derivative (equation (3)) will still serve as a base line against which other expressions for the growth of σ_s will be compared.

10

<u>Norment</u>. The second major formulation of the growth of σ which has achieved a degree of acceptance is put forward by H. G. Norment in "DNAF-1: An Analytical Fallout Prediction Model and Code." He presents a form similar to WSEG-10's formulation with σ_h replaced by the total cloud vertical thickness and the addition of a divisor of 10. Norment's formula is (6:41),

$$\sigma_s = [s_y(z_T - z_B)t_a]/10 \quad (km) \quad (4)$$

where

z_T is the stabilized cloud top,

z_B is the stabilized cloud bottom,

t_a is the time of arrival of the fallout.

Norment states that this equation is "somewhat arbitrary," but "chosen by numerical experimentation to give good comparisons...." (6:44) Equation (4) is taken as the second empirical prediction of the growth of the lateral spread of the fallout pattern against which to compare the results of this study.

Approach

The development of the assumptions necessary to establish a base line are covered in Chapter IV.

Chapter V discusses nuclear cloud formation as presented by WSEG-10 and Hopkins. It also compares the two models and finds the most appropriate one to use for this study.

11

The method of modeling the fall mechanics as they apply to micron sized particles is addressed in Chapter VI. This chapter also includes a description of the "full-physics" computer code used as a benchmark.

Chapter VII shows how the fallout deposited on the ground is treated to determine the characteristic width.

Chapter VIII compares the Norment and WSEG equations to the spread predicted by the model and presents a new derivation by Bridgman which is also compared.

Conclusions and recommendations are presented in Chapters IX and X.

IV. Assumptions

In order to establish a starting point for the study, several assumptions are made. This chapter details those assumptions and justifies them.

1) Local Fallout

Local fallout is hereby specifically defined as that fallout which falls to the earth within the first twenty-four hours following detonation time. This definition is somewhat more restrictive than some. However, as will be shown, one of the major areas of controversy is how the sub-micron size particles interact with the atmosphere. Precisely whether they fall by gravity or are carried by the turbulent atmosphere, sub-micron and even few micron particles are not grounded in 24 hours (7:Ch 2,16). This controversy can be minimized by limiting the calculations to the first twenty-four hours.

It is further assumed that all of the fallout that is present in the initial stabilized cloud can be described by the 100 equal-activity groups determined by Conners as derived from the DELFIC (Defense Land Fallout Information Code) computer code (8:14). Furthermore, any of the particles thus described which are determined to fall to the ground within twenty-four hours will not have been influenced by any buoyant forces inherent in the atmosphere. In summary, the particles of fallout are modeled

13

as spheres, with equal mass radii determined by the DELFIC default spectrum, subject to aerodynamic drag as they fall through the atmosphere.

2) Stratified Atmosphere

The earth's atmosphere is a complex region where many forces interact concurrently, from the earth's surface through the ozonosphere, to create air movement. However, even the most powerful thermo-nuclear weapons (300 megatons) are not thought to be capable of creating clouds that will stabilize above the stratosphere. The troposphere and the stratosphere, then, are the regions of the atmosphere which are of most concern for this study. Within these regions, the temperature, density, pressure, and dynamic viscosity are assumed to be as defined in U.S. Standard Atmosphere (9).

The winds in the troposphere, being easier to measure and of more immediate concern to many researchers, are fairly well documented. Changes in wind speed and direction occur gradually from point to point. The magnitude of the change in wind speed and direction with altitude is defined as horizontal shear. Numerical methods of analysis must represent this smooth change by discontinuous approximations. Available data, as is presented in U.S. Standard Atmosphere, is usually in discrete elements. U.S.Standard Atmosphere uses 50 meters below 11.1 Km and 100 meters for the region between 11.1 Km and 20.0 Km. But, when the magnitudes of shear winds can be found, they are

14

usually reported in 1000 meter increments. As a starting point, it is assumed that a vertical increment of 200 meters gives an adequate representation of shear for the purpose of this analysis. This 200 meter increment is, admittedly, a compromise between the degree of accuracy available by using the same fifty meters as U.S. Standard Atmosphere and the speed of computation which comes from using an increment of 1000 meters.

The stratosphere, by contrast, is considerably less well documented. Even though wind currents appear to be present at all altitudes within the troposphere and the stratosphere, it is often customary to consider the stratosphere to be composed of very large air masses moving essentially geostrophically. These geostrophic winds would negate shear except at the boundaries of the air masses. Thus, some analyses involving the stratospheric winds disregard shear forces completely (10:81). However, since some air movement in the stratosphere can be documented and the precise lower boundary of the stratosphere changes from day to day, this analysis will assume that there is some degree of shear at all altitudes of interest. The magnitude and direction of shear at all altitudes is adressed in greater detail in Chapter VI.

3) Uniform Flat Earth

Inclusion of terrain features in these kinds of models causes each model to predict results which are uniquely defined by the type and size of the included terrain. This makes

comparison between different studies very difficult. Most such studies assume a uniform flat earth.

Additionally, treating the earth's surface as a smooth surface allows the model to continue calculating wind shear effects linearly until downward movement of the fallout has stopped. There are two alternatives to this method. The first alternative is to incorporate the boundary layer turbulence effects for the viscous sublayer (10:155). Such a treatment is difficult and is restrictive to a specific location. The end result is a shortened fall distance and a smaller total fallout pattern. The other alternative is to simply ignore continued shear effects in the region close to the surface. This results in simplifying the calculation but shortens the actual height of fall. The result is the same as if the first alternative is used.

Therefore, the models used in this study assume a uniform flat earth with a constant gravitational field. It is recognized that this assumption causes the resultant fallout pattern to be larger than if surface roughness is included. This increase in the pattern is addressed, and accounted for, during phase three (Chapter VII).

4) Constant Activity

Actual fallout patterns incorporate radioactive decay of the fallout particles during their fall. This is an important feature in calculating radiation doses on the ground. For the

purpose of determining where the activity is, though, the actual amplitude of that activity is unimportant. By working with unit time reference activity, (the activity at 1 hour after burst = $530E10^6$ gamma curies/Kt),the pattern from point to point can be compared directly (2:453).

5) Shear Dominates Only After Three Hours

Torroidal circulation within the expanding cloud is believed to be the dominant effect that continues to expand the cloud from stabilization time until approximately three hours after burst time. This process, although not well understood, is treated by observations of the actual clouds. No attempt is made to calculate the effects of torroidal growth in the model which, thus, does not examine the period from detonation to three hours. It is assumed that torroidal circulation has a negligible effect on cloud growth from three hours on.

V. Phase I - Description of the Stabilized Nuclear Cloud

The assumptions provide the initial framework within which to begin the analysis of cloud growth. This chapter describes the stabilized cloud. Because subsequent full-physics codes use the stabilized cloud as the initial conditions for computing the fall of the individual particles, it is necessary to model the initial cloud as completely as possible.

Approximately five to seven minutes after a surface burst of a one megaton nuclear device, the majority of the upward movement of the particulate matter caught up by the fireball and afterwinds is considered to have slowed sufficiently that the earth's gravity begins to pull the particles back down. Torroidal circulation within the vortex of the cloud continues to affect the location of the particles within the cloud to some extent. This circulation causes continued expansion in both the vertical and horizontal directions until approximately three hours after burst. However, the dominant effect, which causes the upward movement to stop, is the cooling of the material in the cloud to such a degree that it essentially reaches an equilibrium state with the surrounding air. This rise is heavily dependent on the altitude of the tropopause and the heat energy remaining in the cloud at altitude (2:31-32). The upward movement stops while the horizontal torroidal expansion continues. The point in time when this vertical equilibrium state is reached is called the stabilization time.

Compared to the hours which are required for much of the

activity to settle to the ground, the initial six to seven minutes of cloud rise time seem to be negligible. Unless very strong winds prevail throughout the short rise time of the cloud, the cloud rises relatively straight upward along a vertical axis. This study does not look at wind conditions that are strong enough to cause significant movement off this axis. This allows the initial stabilized cloud to be modeled, as shown in Figure 2, with the center axis of the cloud directly over the burst point (also called Ground Zero). The shape of the cloud is modeled as an upright circular cylinder that resembles a tin can. For the moment, the actual dimensions of the cloud remain unspecified.
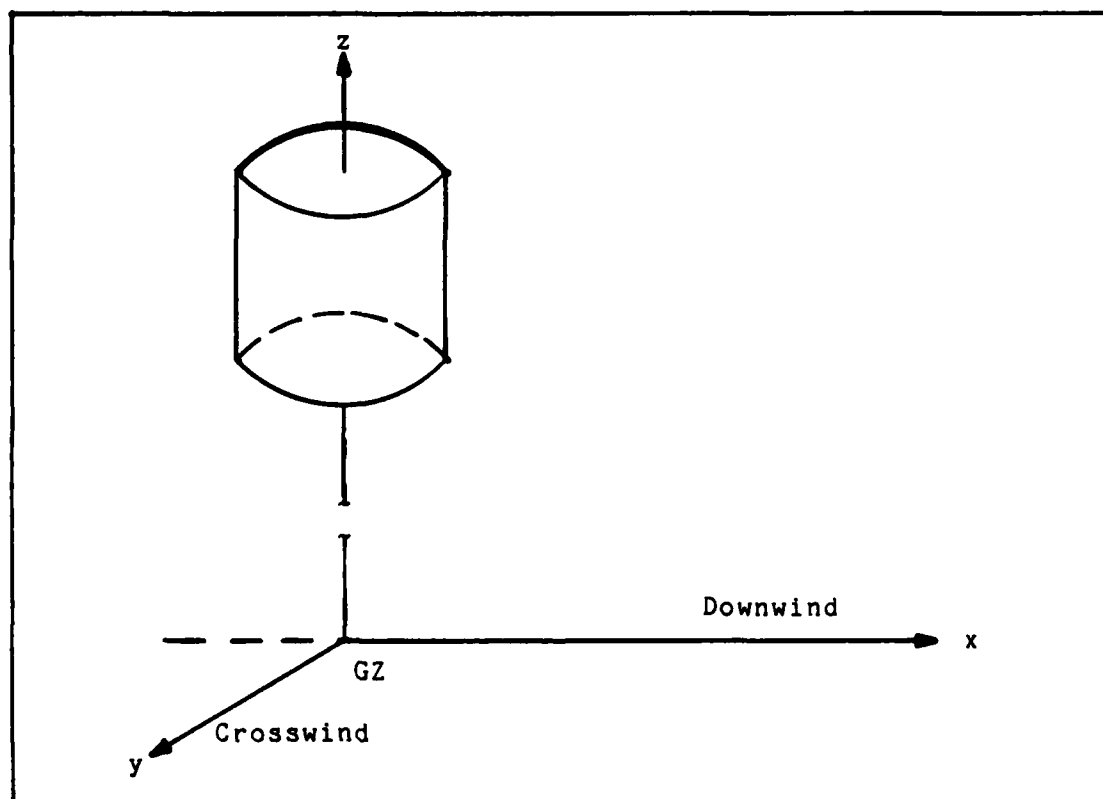
Figure 2. The Initial Cloud Model

19

WSEG's Stabilized Cloud Dimensions

During the writing of WSEG-10, the authors noted that by plotting the activity present in the cloud versus its altitude, as determined from NCTS rocket data, the spatial distribution of activity could be adequately represented by three orthogonal distributions (5:17-19). The three distributions corresponded with the three standard cartesian coordinate axes. By examining each of the three distributions separately, they found that although there were some regions of poor fit, (particularly for the lateral distribution), that there was good enough agreement to consider each distribution to be gaussian (5:21).

The "effective" cloud radius was then defined as "the initial width of the pattern"(5:19) and then by comparison with D.A.S.A. data for the "cloud radius normalized to fit ground zero dose rate" (5:24), they were able to arrive at the following approximation for determination of the characteristic width of the effective initial cloud radius,

$$\ln \sigma_0 = 0.70 + \ln(Y)/3 - 3.25/[4.00 + (\ln(Y) + 5.4)^2] \qquad (5)$$

where

σ_0 is in statute miles

Y is the yield in megatons

Equation (5) has yet to be improved upon and its improvement is not contemplated here.

By examination of the distribution of activity in the

20

vertical direction, G. Pugh and R. Galiano (the WSEG-10 authors) obtained a curve of radioactive cloud center height, h_c, versus yield that could be fit by the following equation (5:24),

$$h_c = 44 + 6.1 \ln(Y) - .205[\ln(Y) + 2.42]|\ln(Y) + 2.42| \qquad (6)$$

where

Y is the yield in megatons

h_c is in kilofeet.

(To avoid confusion, the subscript "0" which is sometimes used in WSEG-10 to indicate the "center" is here replaced by the subscript "c".)

And from the same D.A.S.A. data they concluded that the characteristic vertical width at h_c was,

$$\sigma_z = 0.18 \ h_c \qquad (7)$$

where σ_z and h_c are in kilofeet (3:24).

The lateral component of the orthogonal gaussian distribution simply spreads the total activity, defined by the amplitude of the vertical gaussian at a given altitude, horizontally across the diameter of the cloud at the altitude for which the amplitude was obtained. As with the other two distributions, torroidal circulation affects the size of the area over which this activity fraction is spread. WSEG-10 first uses the assumption that torroidal circulation constricts the initial stabilized cloud width to about half of σ_0. A second assumption that the torroidal effect diminishes to 0, at

21

approximately three hours, is used to achieve some measure of the torroidal growth (5:13-14). However, if the behavior of the fallout pattern near the origin is not significant and if torroidal growth is assumed to be a constant contributor to the overall width of the pattern after three hours, then, when only times after three hours are examined for a determination of growth due to shear, the total contribution due to torroidal circulation can be ignored.

Figure 3, below, is included to assist visualization of the three distributions which describe the initial stabilized cloud according to WSEG-10.
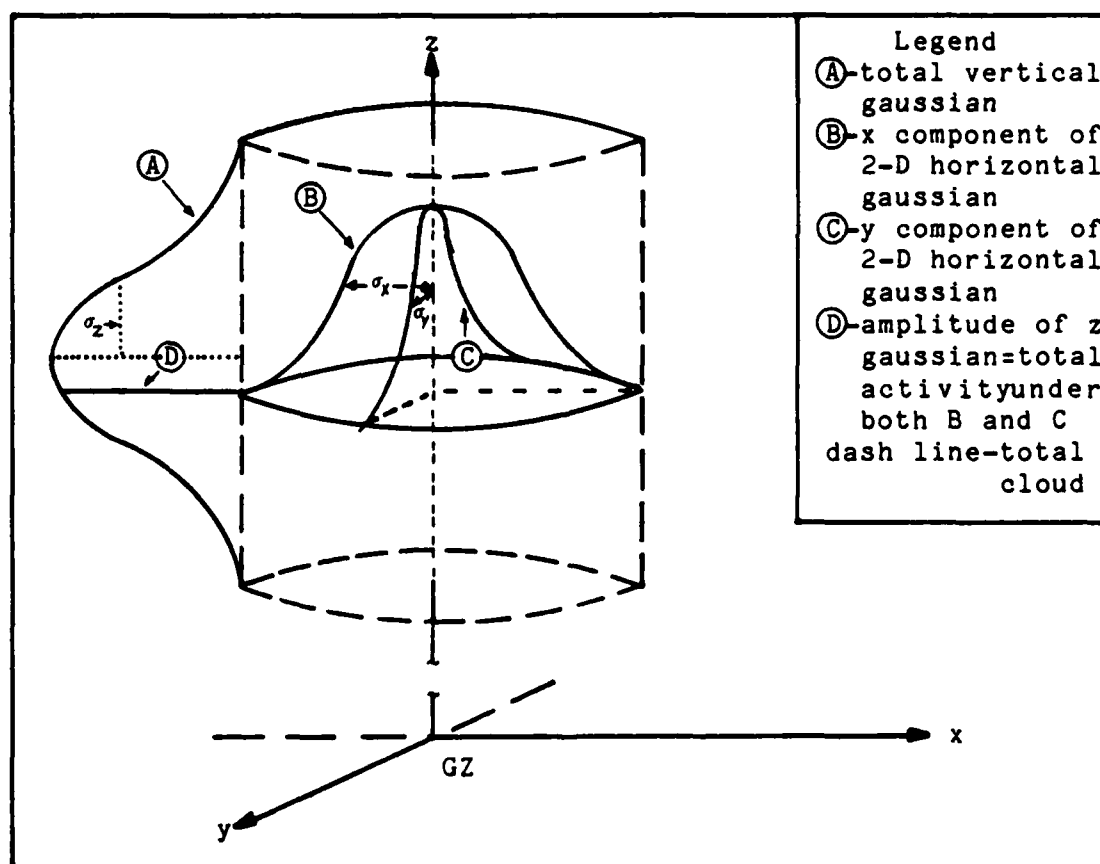
Figure 3. The WSEG-10 Model Stabilized Cloud

It is perhaps interesting to look at what equations (5), (6), and (7) produce for a variety of weapon yields. Table I, below, lists a range of yields and the values WSEG-10 predicts for those yields.

Table I WSEG Predicted Stabilized Cloud Dimensions			
Yield (Mt)	h_c (Km)	σ_z (Km)	σ_0 (Km)
0.17	10.088	1.816	1.485
1	13.043	2.348	2.938
5	15.386	2.769	5.212
9	16.161	2.909	6.394
20	17.145	3.086	8.420
100	18.886	3.399	14.577

Table I lists a 100 megaton yield. As of this writing, it is not believed that such a large warhead is in the inventory of any nation. Using the temperature change as a guide to determining both the top of the troposphere and the top of the stratosphere from U.S. Standard Atmosphere, one can see that the troposphere ends at 11.10 km and the stratosphere at 20.00 km (9:59,61). Other sources allow the stratosphere to extend to as high as 30 km (11:194). However,Table I points out the fact that even the very large yield warheads are still predicted to stabilize within a conservatively estimated stratosphere. Similarly, inspection of Table I shows that, conservatively, a major portion of the radioactive cloud from megaton size weapons will be above the troposphere. It is because of the uncertainty in the precise limits of the troposphere and stratosphere, and the near certainty in stabilization heights as predicted by the

WSEG-10 equations that the second assumption regarding shear in the stratosphere is so important to the determination of σ_S.

Lastly, Table I shows the relevance of using a one megaton yield for this study. Namely, it represents median range values for yield, stabilization height, and cloud radius.

Hopkins' Stabilized Cloud Dimensions

The WSEG-10 model relies heavily on modeling the three spatial distributions as smooth gaussian distributions. The three spatial variables, which are assumed to be independent of each other, can be considered in isolation to determine whether or not they can be improved upon. In the case of the two horizontal distributions, they appear satisfactory, since the early effects of the winds are discounted during cloud formation, and the stratified atmosphere assumes that the distributions will encounter the changing, non-homogeneous medium at all points along the distributions at the same moments during their ascent. Nothing should cause any distortion, then, to the horizontal distributions of activity during cloud rise. The vertical distribution must, however, encounter every non-homogeneity in the atmosphere at succeeding times as it rises and spreads out vertically. This gives rise to the speculation that a more sophisticated model of this process must be utilized.

A. T. Hopkins presented in his thesis, A Two Step Method To Treat Variable Winds In Fallout Smearing Codes, a different method for modeling the vertical distribution of activity in the

24

stabilized cloud (12:14-15). Essentially, the method considers each of the particles defined by the DELFIC 100 equal-activity groups individually and lofts them to altitudes that are dependent on the mass of each particle. This method determines a separate stabilization height for each activity group. A unique σ_z was determined by Conners for the distribution of each activity group in the vertical direction (8:19). The 100 separate distributions add together to form the total vertical distribution.

By running the DELFIC code with yields ranging from 1 Kt to 15 Mt, obtaining a fit of particle size versus altitude with a linear function for each yield as an intermediate result, and then fitting the slopes and intercepts of the intermediate results to polynomials expressed as logarithms of the initial yields, Hopkins (12:14-15) determined that

$$h_0{}^i = I_m + 2r_m{}^i S_m \qquad (m) \qquad (8)$$

where

$h_0{}^i$ is the stabilized altitude of the i_{th} group,

I_m is the intercept of the radius in meters,

$r_m{}^i$ is the mean radius of the i_{th} group in meters,

S_m is the slope of the altitude per meter,

and both I_m and S_m are given by

$$I_m = EXP(7.889 + 0.341 \ln(Y) + 0.001226 \ln(Y)^2$$
$$-0.005227 \ln(Y)^3 + 0.000417 \ln(Y)^4) \qquad (9)$$

$$S_m = -EXP(1.574 - 0.011971n(Y) + 0.036361n(Y)^2$$

$$-0.00411n(Y)^3 + 0.00019651n(Y)^4) \qquad (10)$$

Table II, below, provides a representative sample of what Hopkins' equations produce using the DELFIC 100 equal-activity groups and a yield of 1 megaton. The table is arranged by decreasing radius. Again, the radius is the mean radius of the particles in the group whose total activity comprise one percent of the total activity produced by the 1 megaton explosion. A complete table is presented in Appendix A.

Table II Hopkins' Stabilized Cloud Data							
GROUP	RADIUS (μm)	h_c (km)	σ_z (km)	GROUP	RADIUS (μm)	h_c (km)	σ_z (km)
1	1917.0	0.0*	0.206	55	30.5	13.044	1.934
10	297.0	7.608	1.690	60	24.5	13.167	1.939
20	148.0	10.648	1.826	70	15.4	13.352	1.948
30	89.5	11.841	1.880	80	8.89	13.485	1.954
40	57.5	12.494	1.909	90	4.19	13.581	1.958
50	37.7	12.898	1.927	100	.473	13.657	1.961
*Radii for groups 1-3 produce unrealistic (minus) h_c.							

It is clear that the Hopkins equations produce very similar results to the WSEG-10 equations. This is to be expected. However, by inspection of the 55th group, above, it appears as if the Hopkins model is predicting a cloud wherein the activity is shifted somewhat lower than the WSEG-10 model.

Determining the Best Cloud Model

To determine if there are other significant differences,

26

the two cloud models will be graphically compared. To do this, the WSEG-10 model will be displayed as a vertical gaussian with the median at an h_c of 13.043 km and a σ_z of 2.348 km. Figure 4 displays the WSEG-10 model of the activity of a 1 Mt device versus altitude.

The Hopkins model will be displayed as the sum of all 100 distributions as described by equation (8). Both distributions will be expanded in the horizontal direction to assist in seeing the correlation. The activity will be spread vertically for each group using Conners' development of Hopkins' equations. Conners found that,

$$\Delta z_m{}^i = I_D + 2r_m{}^i S_D$$
$$\sigma_z{}^i 0.25 \Delta z_m \qquad \text{(m)} \qquad \text{(12)}$$

where

$\Delta z_m{}^i$ is the predicted thickness of the i_{th} group,

I_D is the intercept of the radius in meters,

S_D is the slope of the altitude per meter,

$\sigma_z{}^i$ is the characteristic width of the i_{th} group,

and both S_D and I_D are given by

$$S_D = 7 - EXP(1.78999 - 0.048249\ln(Y) + 0.0230248\ln(Y)^2$$
$$-0.00225965\ln(Y)^3 + 0.000161519\ln(Y)^4) \qquad \text{(13)}$$

$$I_D = EXP(7.03518 + 0.158914\ln(Y) + 0.0837539\ln(Y)^2$$
$$-0.0155464\ln(Y)^3 + 0.000862103\ln(Y)^4) \qquad \text{(14)}$$

where Y is the yield in kilotons (8:19).

27
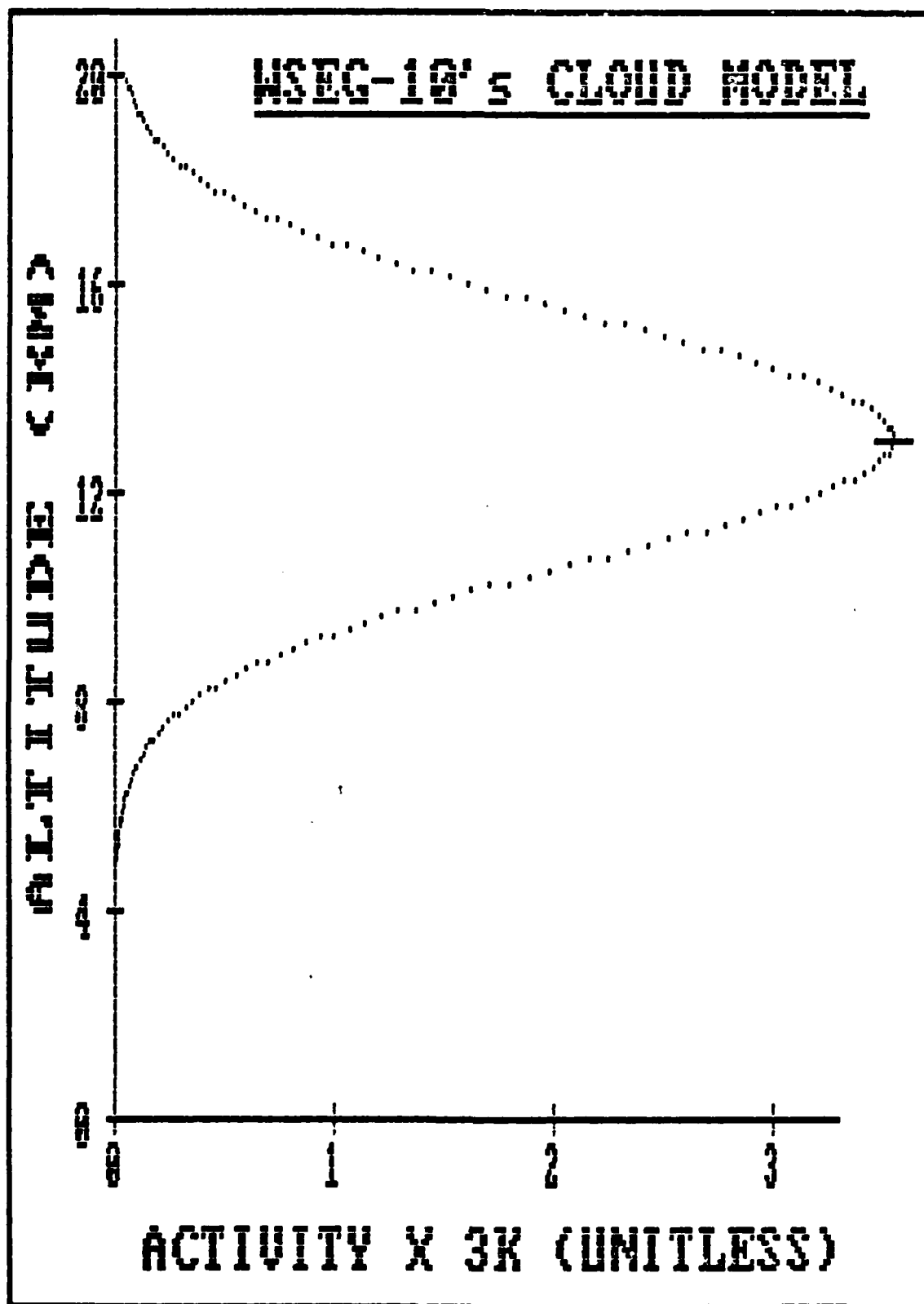
Figure 4. Plot of Activity vs Altitude Using WSEG-10's Model
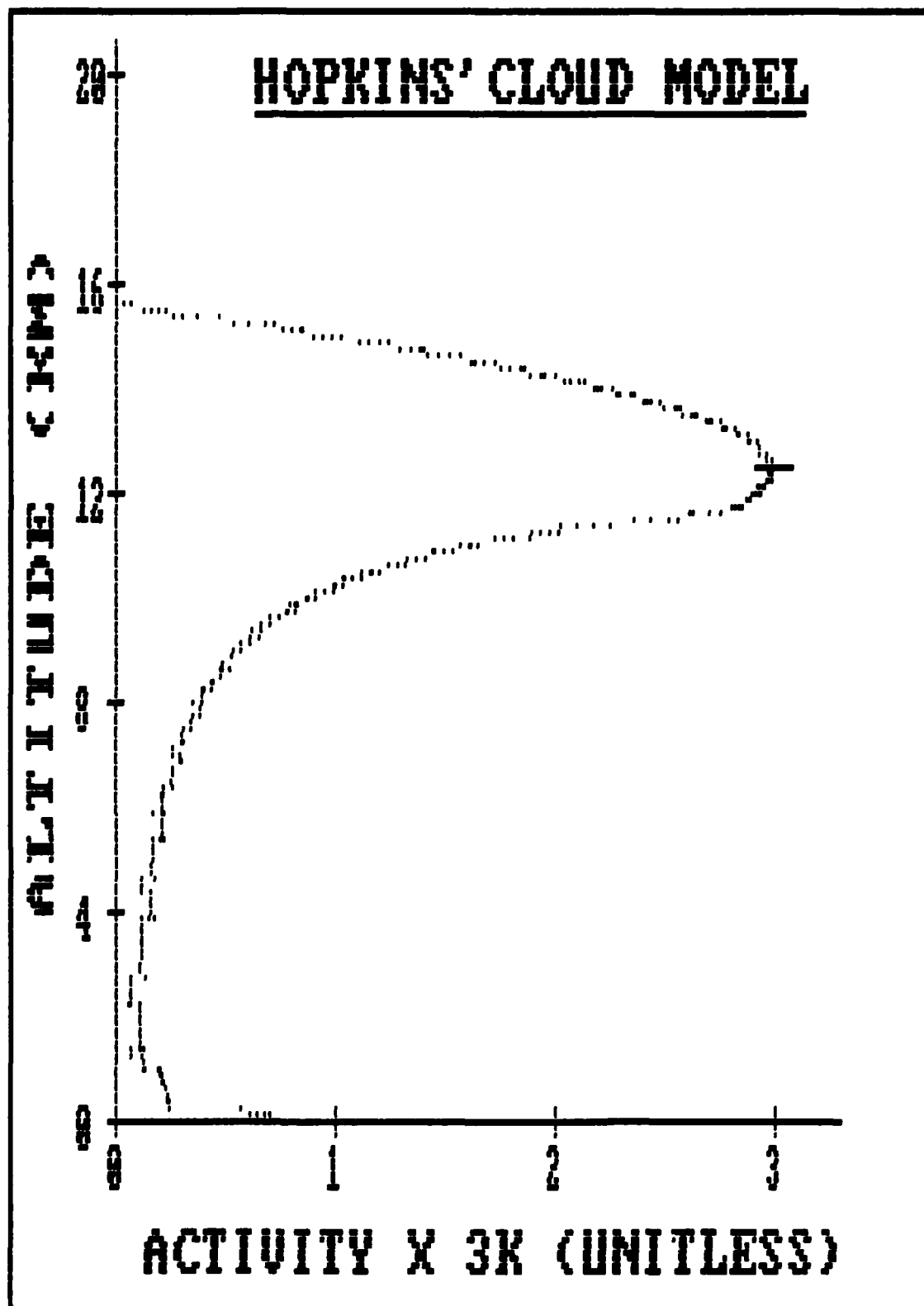
Figure 5. Plot of Activity vs Altitude Using Hopkins' Model

29

By treating the constituent parts separately, Hopkins' model predicts a vertical activity distribution which more closely approximates the overall shape of the activity-plot derived from NCTS rocket data, presented by WSEG-10, than does the single Gaussian approximation using the WSEG-10 model. Therefore, it is believed that the Hopkins model for vertical activity is better than the WSEG-10 model. WSEG-10's model for lateral spread, for the reasons stated previously, remains the best model for the other spatial distributions.

It is cumbersome to deal with the 100 different characteristic widths associated with Conners' technique. To simplify the model, the plot of activity versus altitude from Hopkins (Figure 5) is fit to the WSEG-10 plot (Figure 4). This is done byholding the area under the Hopkins plot constant and increasing σ_z until the three inflection points on both curves coincide. (See Figure 6). These three inflection points define $\sigma_{z(B)}$ forthe bottom half of the plot, the peak or maximum horizontal extent,and the $\sigma_{z(T)}$ for the top half of the plot. The values of the two σ_z are not expected to be the same since the plot is clearly skewed, but they should be similar. Also, because the simplification will be defined by only one σ_z, fitting the two plots together produces an area of underlap in the lower altitudes and an area of overlap in the upper altitudes. However, the central portion of the Hopkins plot can be brought into coincidence with the WSEG-10 plot. The overall σ_z that produces this coincidence is the desired σ_z that best

30
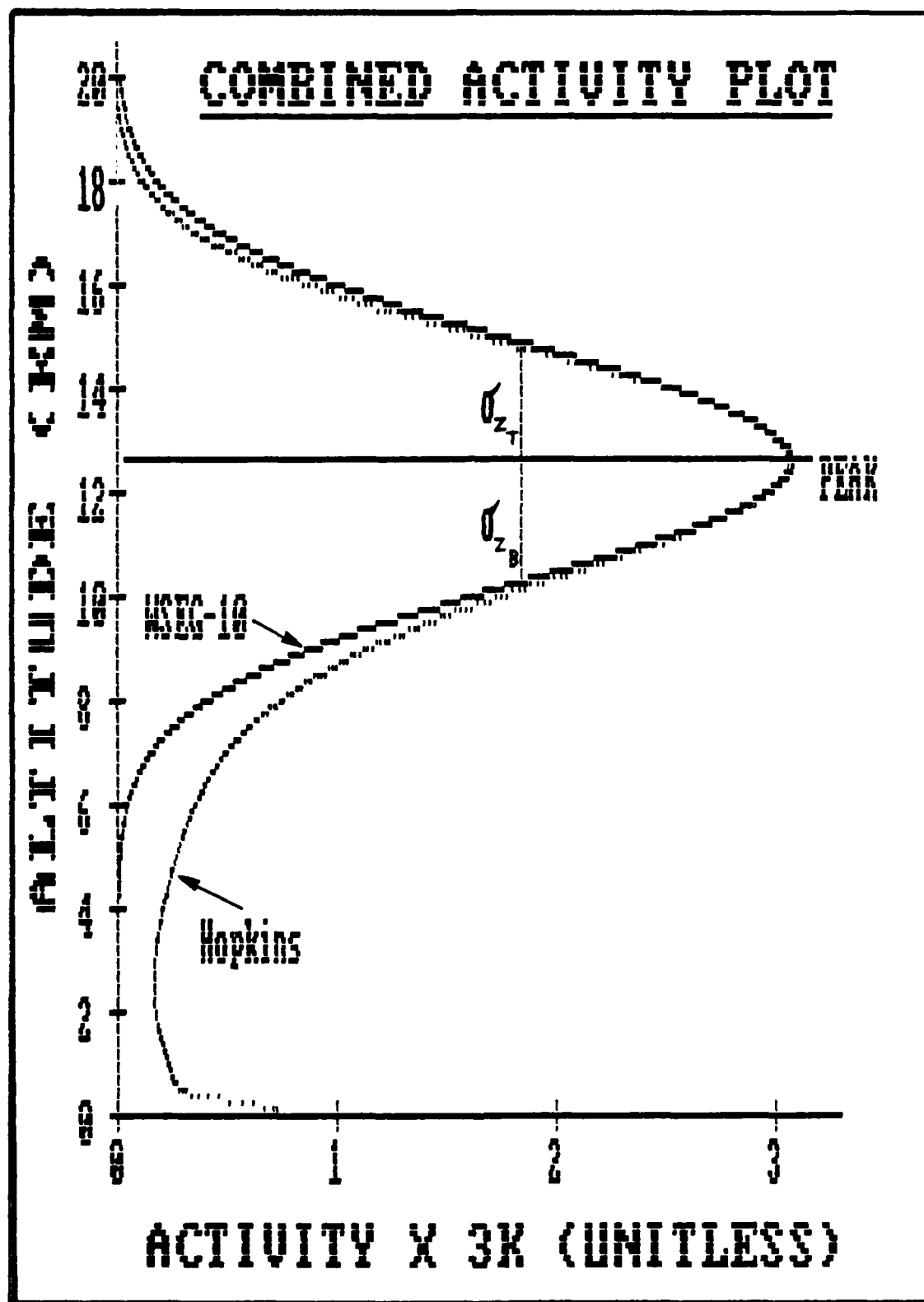
Figure 6. Superposition of WSEG-10 and Hopkins Plots

31

describes the fitted, simplified Hopkins model for vertical activity. The σ_z that produces the degree of fit evident in Figure 6 is 2.28 km.

This completes the model that establishes the initial conditions for the nuclear cloud. The fallout particles fall to the ground from their initial spatial positions as defined by two WSEG-10 lateral Gaussian distributions and one Hopkins vertical distribution with an ammended σ_z of 2.28 km.

VI. <u>Phase</u> <u>II</u> - <u>Fallout</u> <u>Transport</u> <u>in</u> <u>the</u> <u>Atmosphere</u>

A single object falling through the atmosphere is relatively easy to follow without the use of computers. When large numbers of objects are being followed, a computer is obviously more appropriate. As the study of fallout involves many particles, it is only natural that several well defined computer code types have evolved. The two most common types are the "Smear" code and the "Disk Tosser." Of these two types, the disk tosser is more adapted to following the specific path taken by a particle as it falls.

A disk tosser begins with a set of discrete radii particles representing an equal mass subdivision of the particle size distribution. Each particle has a vertical coordinate which uniquely defines its location. The cloud model, as parameterized in the preceding chapter, is this set of coordinates. Each of the 100 particles, then, is represented by an initial starting altitude. A disk is formed by taking the characteristic width of the cloud center at stabilization and using it as the radius of the disk. The amount of activity contained in the disk depends on its distance from the median of the vertical distribution used to define the vertical activity. Because the effects of wind are ignored prior to stabilization, there is no initial lateral translation of the disk from the vertical axis. The disk tosser then applies whatever wind conditions are considered appropriate, "tosses" each disk into the wind field, and the operator observes where the disk goes. A simple analogy might be

to consider each disk as an infinitely thin frisbee thrown by a mechanical arm at a predetermined height. Clearly, the design of the wind field has a large impact on the path of the disk. This is now examined in more depth.

Modeling the Winds

The "X" Wind. By definition, the direction of the X wind is the direction of the wind at the cloud center stabilization altitude. The direction at h_c is deliberately chosen as the downwind direction because the disk that starts its fall from h_c will have the maximum amount of activity. By observing the locations of all the disks that started from h_c, a line of maximum activity can be traced on the ground. This line is referred to as the "Hotline."

In the simplest case, where there are no crosswind components, the hotline and X axis are identical. If a crosswind component other than zero is chosen, the hotline and the X axis will diverge from a common origin, i.e. ground zero.

The wind speed at h_c is only critical in that it must be non-zero. Clearly, a zero downwind velocity would cause no translation in the downwind direction. Likewise, any positive non-zero velocity will translate the fallout in the downwind direction according to the following equation,

$$t_a v_x = x \tag{15}$$

34

where

t_a is the time of arrival,

v_x is the downwind wind velocity, (previously W)

x is the downwind translation.

Again, since the spatial variables are independent of one another and the downwind translation as shown by equation (15) is not a function of Y, the downwind wind velocity can be ignored.

The "Z" Wind. The stratified atmosphere assumption allows uniform treatment of the effects of air density on fall velocity with altitude. Inclusion of a wind with a Z component alters the composition of the atmosphere as related by U.S. Standard Atmosphere. WSEG-10 chooses to ignore vertical winds by concluding that the transport is "... primarily horizontal not vertical." (5:3) More specifically, defining a non-zero vertical wind causes the otherwise independent spatial variables to lose their independence. Panofsky and Dutton suggest that even in the more complex applications, where precise expressions of three dimensional wind fields are desired, the three variables are treated independently (13:230-235). Therefore, vertical winds are not treated by this model.

The "Y" Wind. The "Y" wind, or crosswind, acts on the particles in a direction normal to the downwind direction. Since the direction of the wind at h_c is defined as the downwind direction, the magnitude of the normal, or Y component of the wind at h_c must be zero. The magnitude of the crosswind is known

35

to change with altitude. A typical value of the change lies between 1.0 and 10.0 km/hr-km of altitude. It is this change in magnitude with altitude that is defined as horizontal shear. Two examples are used, next, to assist in refining the range of shear values to a single value to be used in the model as an average shear.

Actual Observations. On 5 July 1957, in the Nevada desert, a 74 Kt device was exploded as the final portion of Operation Plumbbob Hood. Table III represents a portion of the wind data recorded at H-hour. Figure 7 is a top-down view of the data from Table III with all the wind vectors acting at, or directly above, the origin. By averaging the change in wind speed from the surface to cloud top, one can see that the average shear is 6.32 km/km-hr. Initially, this appears to be a valid shear value since it lies within the range of typical shear values shown above. However, since the cloud is the result of only a 74 Kt yield device, the cloud top does not project beyond the tropopause. The shear values in Table III naturally reflect the greater turbulence of the troposphere.

The second example, provided by the Air Force Operational Test and Evaluation Center (AFOTEC), helps to clarify whether the average shear developed from the first example is too high or not.

AFOTEC Wind Projections. AFOTEC has a data file of observed winds at various pressure heights for a 5 by 2.5 degree grid that spans the globe. Accessing this data file for the wind

36

Table III

Nevada Wind Data for 5 July 1957
Site elevation - 4230 ft : 37° 08' N, 116° 02' W

Altitude[1] #	(k-ft)	Angle (deg)	Speed (mph)	Del V[4] (mph)	Altitude #	(k-ft)	Angle (deg)	Speed (mph)	Del V (mph)
1	ground	calm	0	5	12	26.0	220	10	6
2	6.0	200	5	4	13	28.0	190	14	4
3	8.0	180	9	3	14	30.0	200	24	10
4	10.0	160	12	2	15	32.0	210	26	2
5	12.0	150	14	2	16	34.0	220	21	-5
6	14.0	270	23	9	17	36.0	220	25	4
7	16.0	180	33	10	18	38.0	210	23	-2
8	18.0	180	24	-9	19	40.0	210	26	3
9	20.0	180	12	-12	20	42.0	210	28	2
10	22.0	220	9	-3	21	44.0	220	36	8
11	24.0	230	13	4	22	46.0	220	39	-

notes: 1. All altitudes are with respect to Mean Sea Level.
2. Cloud top - 48000 ft: Cloud bottom - 35000 ft.
3. Tropopause height measured at 53149 ft.
4. Change in speed to next higher altitude.

(14:280-283)

Scale: 1" = 5 mph
note: Number at vector head refers to item (#) above.
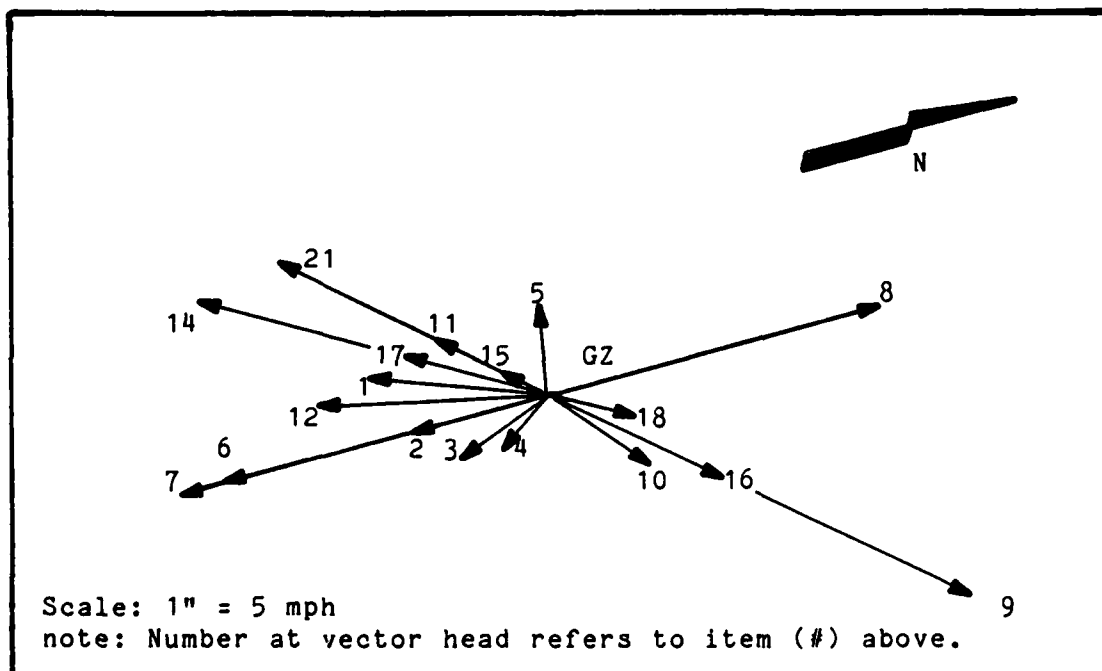
Figure 7. Observed Nevada Shear above Ground Zero

37

data that most closely matches the date and geographical location of the Plumbbob test produces the data shown in Table IV for 16 July. (The data represents five year averages of observations and, thus, is not tied to a particular year.) This data is depicted in Figure 8 in the same manner that was used for Figure 7. The average shear is found to be 0.18 km/hr-km. The last two pressure levels shown in Table IV reflect altitudes that are above the tropopause as measured on 5 July 1957. The last pressure level (70 mb) is clearly within the stratosphere. Here, the magnitude of the wind has fallen sharply from the levels it was at in the troposphere. This drop in magnitude is a contributor to the lower average shear value.

Although no direct comparison of these two examples can be made, they can be used to help bound the appropriate value of average shear for the model. The observed data covers the winds in the troposphere in detail for one specific day. The predicted data from AFOTEC is an average of five days and extends to a greater height than the observed data. The "best" value lies between the two.

The WSEG-10 authors use a shear that ranges from 0.1 to 0.4 knots/1000 ft. A comment is made that these shear values are more common at 50 k-ft and, that at a lower altitude of 30 k-ft, higher shear values are found (5:47). Both for ease of comparison with WSEG-10 results and as a median value of the shear values discussed above, this study uses 1.0 km/km-hr as the effective shear for all altitudes. A 200 meter increment of

38

Table IV

AFOTEC Projected Wind Data for Nevada : 37o N, 117.5o W
(16 July of any year)

Item #	P [1] (mb)	Y [2] (km/hr)	X [3] (km/hr)	Altitude (k-ft)	Angle[4] (deg)	Speed (km/hr)	Del V[5] (km/hr)
1	850	5.5512	12.9528	4.757	66.8	14.09	14.63
2	700	27.7560	7.4016	9.843	75.1	28.72	0.01
3	500	- 7.4016	27.7560	18.373	104.9	28.73	- 8.04
4	400	3.7008	-20.3544	23.622	280.3	20.69	30.62
5	300	22.2048	-46.2600	30.184	334.4	51.31	-28.42
6	250	-22.2048	5.5512	34.121	104.0	22.89	13.56
7	200	33.3072	14.8032	38.714	66.0	36.45	- 0.90
8	150	-27.7560	-22.2048	44.619	218.7	35.55	- 3.23
9	100	-29.6064	12.9528	53.150	156.4	32.32	-16.62
10	70	11.1024	-11.1204	60.696	315.0	15.70	-

notes: 1. Pressure
2. Y component of the wind
3. X component of the wind
4. Not corrected for deviation from magnetic north
5. Change in speed to next higher altitude

(15)

Scale
1" = 10 km/hr

note: Number at vector head
refers to item (#) above
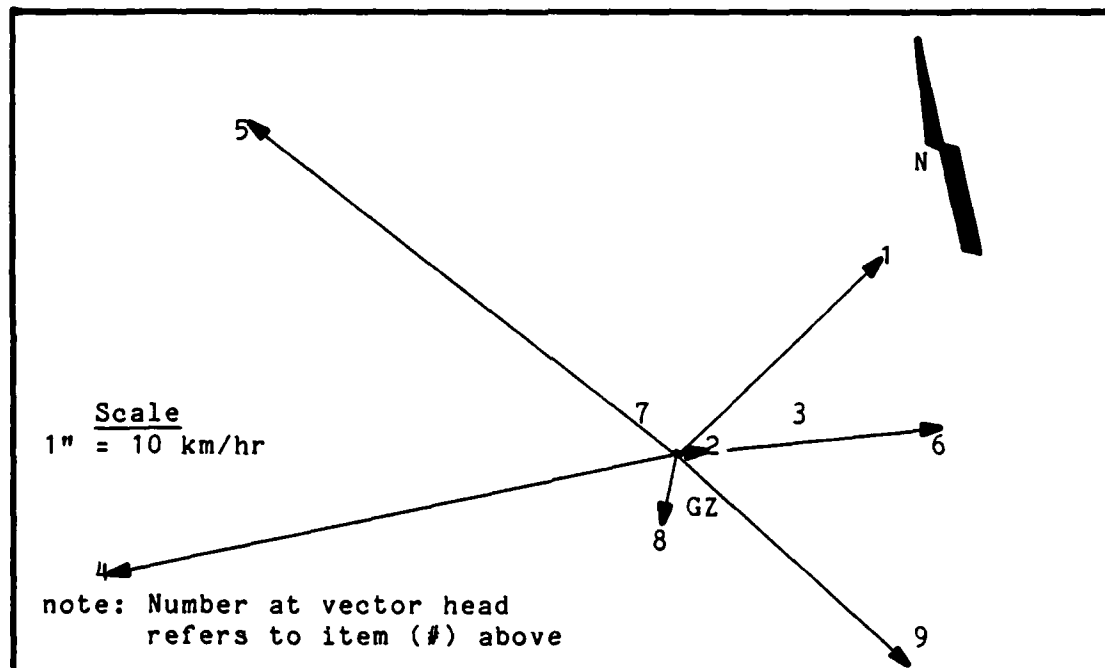
Figure 8. Predicted Shear for Operation Plumbbob

altitude and 0.2 km/200 m-hr allows a smoother transition of wind velocity with altitude than does the 1.0 km/km-hr shear value.

Finally, both the actual shear data and the predicted shear data demonstrate the large variability in direction at different altitudes. A particle subject to this variation would find itself moving back and forth as it fell to the ground. The crosswind distancetravelled is, therefore, less than if the crosswind were from only one direction. The maximum total influence of the crosswind is achieved by allowing it to act on the fallout, in the same direction, at all altitudes. To model this maximum extent, and yet still constrain the value of shear at h_c to 0.0, a convention is established that defines the shear above h_c as acting in the negative direction and below h_c as acting in the positive direction with respect to the Y axis. Figure 9 illustrates how this convention operates in two dimensions to produce a discrete yet continuous crosswind magnitude in a case where h_c is 13.0 km.

The last group of parameters with which the model must contend describe the downward motion of the particles. These forces must be balanced to produce a realistic time and speed of fall.
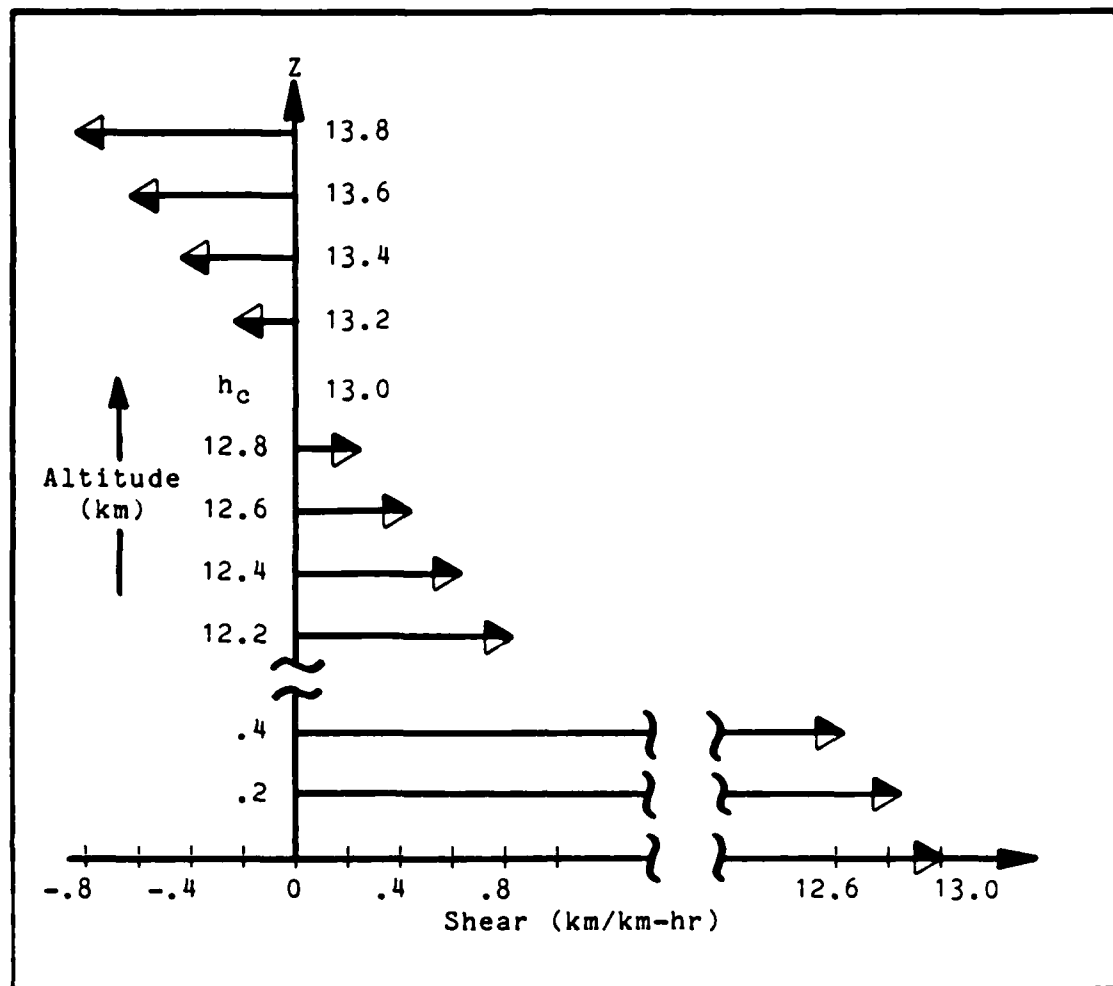
Figure 9. Maximum Shear Effect Model

The Fall Mechanics

Each particle of fallout must remain in the layers of the stratified atmosphere for a finite amount of time in order for the crosswind to have an effect. Considering a particle at a specific time within its total fall time, leads to a static condition where all the forces acting on the particle are in balance. For the moment, the lateral forces exerted by the crosswind will be ignored. This leaves only the vertical forces.

41

It is possible to approximate the forces by beginning with a term for the buoyant force as

$$F\uparrow = P_D C_d \sigma \qquad (16)$$

where

$F\uparrow$ is the upward force (N),

P_D is the dynamic pressure (kg/m-sec^2),

C_d is the drag coefficient (dimensionless),

σ is the cross sectional area (m^2).

And, the downward force is simply

$$F\downarrow = Wg \qquad . \qquad (17)$$

where

$F\downarrow$ is the downward force (N),

W is the mass of the particle (kg),

g is the gravitational constant (m/sec^2).

The assumption that all of the fallout particles are spheres allows some simplification of the above equations as follows: the dynamic pressure on a sphere is $P_D = (1/2)\rho_a v_z^2$; the cross sectional area of a sphere is $\sigma = \pi r_2$; and the mass is $W = (4/3)\pi r^3 \rho_f$. For the forces to be balanced, $F\uparrow$ must equal $F\downarrow$. Setting them equal and making the substitution, one gets

$$(1/2)\rho_a v_z^2 C_d \pi r^2 = (4/3)\pi r^3 \rho_f g \qquad (18)$$

where

ρ_a is the density of the air (kg/m^3),

v_z is the velocity of the particle (m/sec),

r is the radius of the particle (m),

ρ_f is the density of the fallout (2600 kg/m^3).

From equation (18) one could solve for the velocity by rearranging the terms and substituting the correct values for ρ_a and C_d. Unfortunately, C_d is a derived value based on the fall velocity of the particle and the particle's shape. Fortunately, by combining the work of Davies and McDonald, as presented by Bridgman and Bigelow (16:212), the drag coefficient can be treated in such a manner as to eliminate the need to solve for C_d explicitly. Davies shows two relationships (equations (19) and (20)) between C_d and Re (Reynolds number) and, Davies shows a relationship (equation (21)) between Re and v_z (17:463). These relationships are,

$$Re = Re^2 C_d/24 - 2.3363 E10^{-4}(Re^2 C_d)^2$$
$$+ 2.0154 E10^{-6}(Re^2 C_d)^3 - 6.9105 E10^{-9}(Re^2 C_d)^4 \quad (19)$$
$$\text{for } Re^2 C_d < 120$$

$$\log(Re) = -1.29536 + 0.986\log(Re^2 C_d) - 0.046677[\log(Re^2 C_d)]^2$$
$$+ 0.0011235[\log(Re^2 C_d)]^3 \quad \text{for } Re^2 C_d >= 120 \quad (20)$$

where Reynolds number is defined as;

$$Re = (2v_z r)/\nu \quad (21)$$

43

where ν is the kinematic viscosity of the air (m^2/sec). However, since $\nu = \eta / \rho_a$ the Reynolds number can be restated as

$$Re = (2v_z \rho_a r)/\eta \qquad (22)$$

where η is the dynamic viscosity of the air (kg/sec-m). Solving equation (22) for v_z yields

$$v_z = Re\eta/(2\rho_a r) \qquad (23)$$

and substituting this into equation (19) McDonald obtains (17: 463)

$$Re^2 C_d = (32\rho_a \rho_f g r^3)/(3\eta^2) \qquad (24)$$

Now, the quantity $Re^2 C_d$ is defined by parameters which are known. $Re^2 C_d$ can be used in equations (19) and (20) to determine Re. With Re defined, equation (23) becomes an expression for the instantaneous velocity at a given altitude. A correction factor for high altitude "slip" is suggested by Davies. Here the correction factor used by DELFIC, as reported by Bridgman and Bigelow (16:212), is used. It is

$$CF = 1 + 1.165E10^{-7}/(r\rho_a) \qquad (25)$$

The final expression for the balanced forces on the fallout as it falls is, then,

$$v_z = (CF)Re\eta/(2\rho_f r) \qquad (m/sec) \qquad (26)$$

44

An Expression for Fall Time

Equation (26) expresses the velocity at a specific altitude. In order to arrive at an equation that expresses the time of fall, a few additional steps must be taken. Since, in general,

$$(velocity)(time)=distance$$

if the distance is the total height from which the particle must fall and velocity is the velocity in the z direction, then

$$v_z t = z \qquad (27)$$

and

$$t = \Delta z / v_z \qquad (28)$$

and, if rather than take the entire height of fall, one takes z (in equation (28)) to be an increment of altitude, and the velocity is assumed constant over this increment of altitude, then,

$$t = \Delta z / v_z \qquad (sec) \qquad (29)$$

where

  t is the amount of time to fall through Δz,

  $\Delta z = 200$ m,

  v_z is defined by equation (26) (m/sec).

If equation (29) provides the time of fall through one increment

45

of altitude, then adding the times from all the increments gives the total time of fall. The total time of fall is, clearly, the time of arrival of the particle on the ground, and it is referred to as t_a. Stated another way,

$$t_a = \sum_{i=1}^{n}(\Delta z/v_z^i) \qquad (\text{sec}) \qquad (30)$$

By combining equation (29) and the shear force at each altitude, the lateral translation of the particle is determined. Ultimately, as the particle is transported through the lowest increment of altitude and is translated by the final shear force, the particle arrives at its "grounded location."

Figure 10 is a graphical representation of these balanced *forces with a time history of a hypothetical particle.* So that the mechanism is more readily visible, the particle is only lofted to a height of 6 km. Cloud center stabilization altitude is chosen to be 4 km so that the effect of the shear convention above h_c, in the negative direction, is more apparent. The horizontal shear is 1 km/km-hr. For the purpose of this illustration only, the atmosphere is considered to be homogeneous so that the fall velocity, v_z, becomes constant. The showing of the "fall distance" arrow as a force vector is merely an artifice to assist visualization. The "effective wind" is any arbitrary non-zero wind with units of km/hr. A "track" in the X-Y plane is the ground projection of the "path travelled." This is representative of what the computer code is actually storing as the lateral distance of the particle from the downwind axis.

46
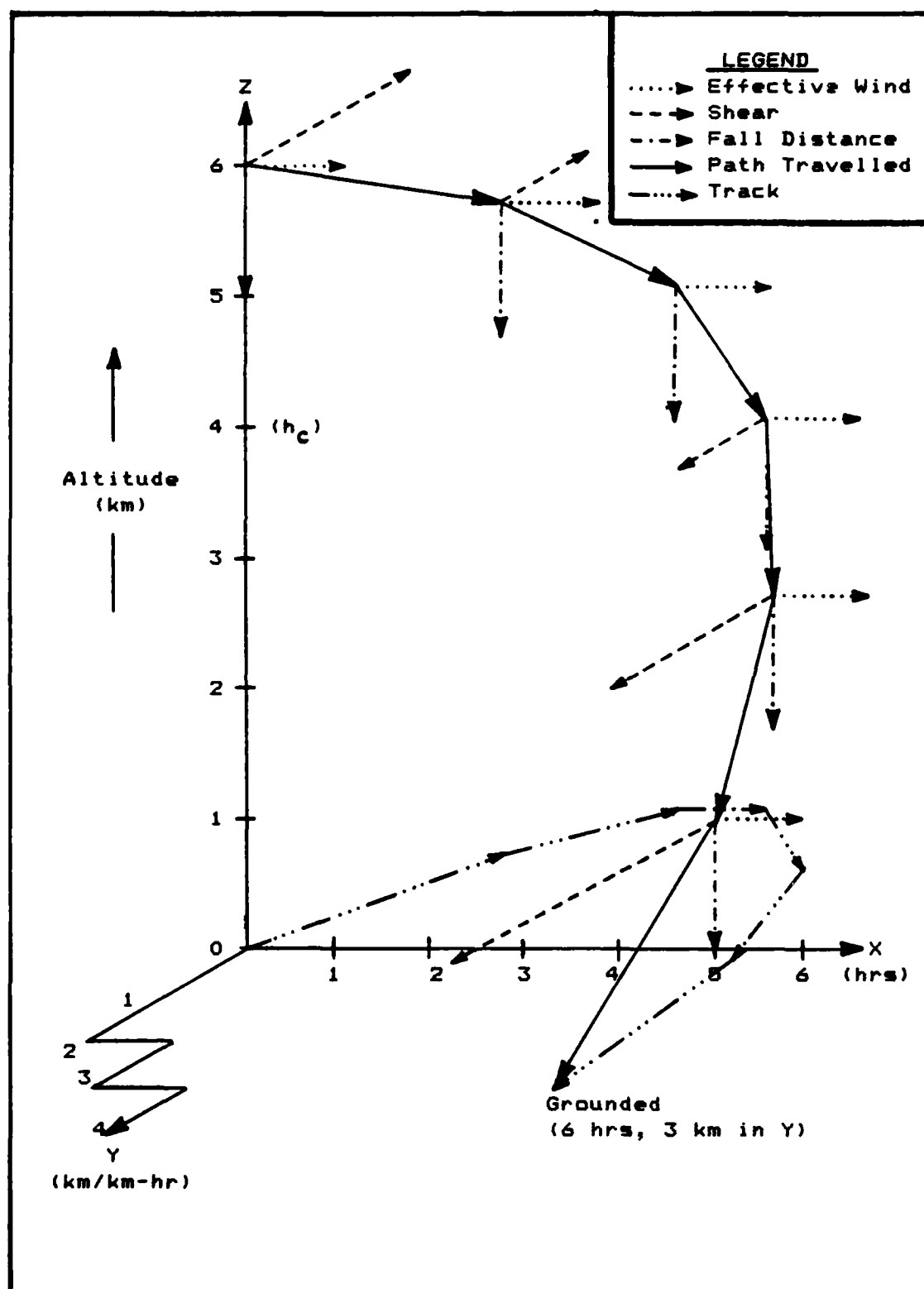
Figure 10. The Transport Model in Operation (Simple Case)

47

With a set of values placing a particle in the cloud model as an initial condition, the transport model operates to determine that particle's grounded location. The third phase of pattern formation requires the grounded location of all the particles to be determined. However, before this phase is discussed, some intermediate results from the examination of just one or two particles will be discussed.

Intermediate Results

The interface between the cloud model and the transport model is accomplished by use of Colarco's equation and coefficients (18:11,67-71). Colarco shows that by replacing the vertical distribution by a Dirac delta function, the following equation predicts the particle size that arrives at t_a.

$$r = \sum_{i=1}^{6} C_i t_a^{i-6} + C_7 t_a^{-.5} \qquad (\mu m) \qquad (31)$$

where C_i and C_7 are the coefficients from Colarco's work and t_a is in hours. When the coefficients for an altitude of 13 km are used, the resultant radii define those particles that originated at h_c. This is particularly useful for determining the location of the hotline. Furthermore, with all of the activity of the disk confined to the Dirac function, rather than distributed under a gaussian curve, the deviation of the grounded location in this case from the downwind axis is the translation due to the shear.

48

In the process of applying Colarco's equation to determine an initial set of data points defining the hotline for a stabilization altitude of 13.04 km and times from 3 to 24 hours, it was decided to perform a secondary calculation using the transport model. The radius predicted by equation (31) was entered into equation (30). Both equation (30) and (31) should have yielded the same t_a. As can be seen in Table V, the Colarco predicted radius was found to be slightly different than the radius required by equation (30) to achieve the same t_a. This discrepancy was not resolved. Colarco used a polynomial fit routine to determine the coefficients. Because of this method, it is believed that some degree of error was introduced to the coefficients. Therefore, equation (30) was thought to be more accurate. Colarco's method proved to be a quick way of approximating the correct radius. The Colarco prediction was then incrementally adjusted until the radius, after substituting into equation (30), produced the desired t_a.

As stated previously, the downwind wind velocity is not critical. Merely as a point of reference, Table V shows the downwind translation using a v_x of 50 km/hr.

Just as the particle originating from h_c defines the hotline, so also does the hotline define the center of the lateral distribution on the ground in the Y direction when the activity is not constrained by a Dirac function. This follows from the assumption that the vertical distribution, which is

49

approximated by the gaussian distribution, is translated to a gaussian distribution in Y. Subsequently, a particle which is defined as being a distance σ_z from h_c will, after being transported to the ground, be a distance defined by σ_y from the hotline. The importance of the shape and location of the hotline, then, is sufficient to warrant a closer look.

Figure 11 shows the predicted locations of the hotlines formed by shears of 0.2, 0.6, and 1.0 according to the data listed in Table V. Clearly, in the regime from 3 to 24 hours, when only the translation due to shear is considered, the hotlines project as straight lines.

Following the same procedure that was used to determine the hotlines, the grounded locations of the particles that

50
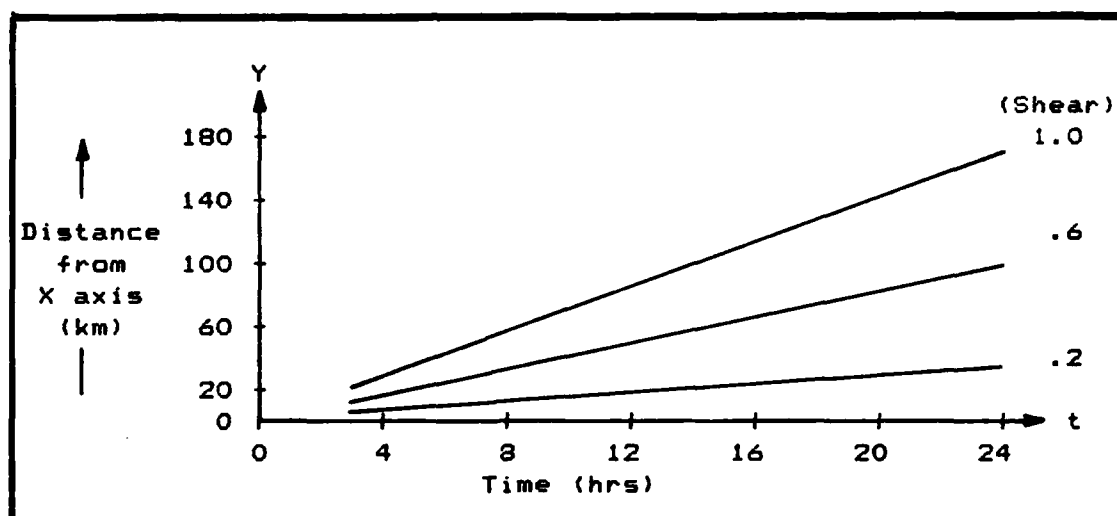
Figure 11. Predicted Hotlines for 3 Shear Values

originate at $h_c + \sigma_z$ are shown in Table VI.

The lateral separation in the Y direction, between the locations for the particles which started at h_c and the particles which started at $h_c + \sigma_z$, is σ_y. Table VII lists the

Table VI							
Locations of Particles from $h_c + \sigma_z$							
t_a (hr)	r_c (μm)	r_m (μm)	Y (km) [for various shear]				
			.2	.4	.6	.8	1.0
3	81.70	81.22	3.80	7.61	11.41	15.22	19.02
4	66.71	65.64	5.04	10.07	15.11	20.15	25.19
6	51.01	49.90	7.41	14.82	22.24	29.65	37.06
8	42.55	41.89	9.86	19.72	29.59	39.45	49.31
10	37.10	36.62	12.29	24.58	36.87	49.16	61.45
12	33.22	32.89	14.68	29.36	44.05	58.73	73.41
14	30.30	30.11	17.07	34.13	51.20	68.27	85.33
16	27.99	27.94	19.44	38.88	58.33	77.77	97.21
18	26.11	26.18	21.83	43.65	65.48	87.31	109.14
20	24.54	24.72	24.21	48.42	72.63	96.84	121.06
22	23.20	23.48	26.59	53.18	79.77	106.37	132.96
24	22.05	22.42	28.97	57.94	86.91	115.88	144.85
note: All shear have units of km/km-hr.							

Table VII σ_y Values for 5 Shear				
t_a (hr)	.2 (km)	.4 (km)	.6 (km)	.8 (km)	1.0 (km)
3	.580027	1.16005	1.74007	2.32001	2.90013
4	.788387	1.57678	2.36516	3.15354	3.94193
6	1.23034	2.46067	3.69101	4.92135	6.15168
8	1.65997	3.31993	4.97989	6.63986	8.29983
10	2.07494	4.14989	6.22484	8.2998	10.3747
12	2.51727	5.03454	7.55181	10.0691	12.5864
14	2.96347	5.92694	8.89041	11.8539	14.8173
16	3.41088	6.82175	10.2326	13.6435	17.0544
18	3.84931	7.69863	11.5479	15.3972	19.2466
20	4.29521	8.59043	12.8856	17.1808	21.4760
22	4.75827	9.51655	14.2748	19.0331	23.7913
24	5.18831	10.3766	15.565	20.7533	25.9416
note: All shear in units of km/km-hr					

Figure 12. Plot of σ_y versus Time

52
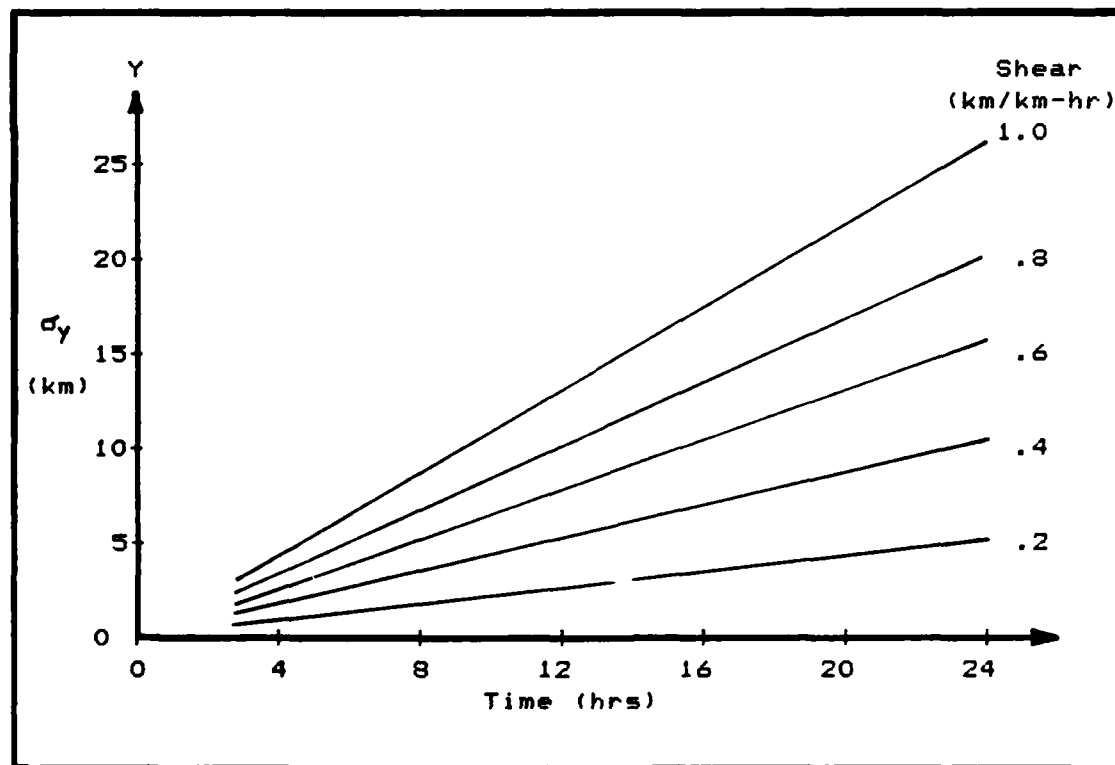
computed difference between the locations for the five values of shear used for Tables V and VI. Figure 12 is a plot of these σ_y.

Before attempting to look at the patterns formed by all the particles, the vertical increment of fall distance will be analyzed in an effort to ensure that it is the most appropriate one to use for the completed computer model.

Variations of the Δz Parameter

The Dirac function substitution provides a quick method of testing one of the primary assumptions. The use of 200 meters as the "best" increment of vertical distance is used both for the shear increment and the fall distance over which the fall velocity is held constant. A comparison of this parameter establishes the validity of this assumption.

Table VIII shows the results of varying the vertical increment, Δz, from 1000 m to 50 m. 50 m is considered to be the most accurate increment available because the parameters defining v_z, from U.S. Standard Atmosphere, are not given in any finer detail. Therefore, the time of fall that is computed using Δz = 50 m, is assigned a degree of accuracy of 100%. The other Δz are compared to the 50 m fall time and assigned a relative degree of accuracy accordingly.

Deciding which Δz to use is largely subjective. However, Table VIII demonstrates that the primary assumption, that 200 m is sufficiently accurate to predict valid results, is a correct one. The most accurate result is achievable with Δz = 50 m, but

53

at a cost of a computer program that is 4 times longer to run than if Δz is taken as 200 m. Considering the desire to develop a calculational method that was relatively quick and still retained a high degree of accuracy, it is believed that the 0.27% loss of accuracy from using a Δz of 200 m, is completely satisfactory.

This completes the discussion of the transport of the fallout particles through the atmosphere. When the computer model operates on the entire cloud, rather than just one or two particles, the resulting grounded locations form the fallout pattern. This pattern, and its analysis, are discussed next.

Table VIII			
Comparison of Fall Times Developed from Different Δz			
z (m)	Time (hrs)	% Accuracy [1]	Run time [2]
1000	2.89451	98.31	1
500	2.92063	99.20	2
200	2.93634	99.73	5
100	2.94158	99.91	10
50	2.9442	100.00	20
notes: 1. Related to Δz = 50 m 2. Arbitrary units			

VII. Phase III - The Grounded Fallout Pattern

The grounded fallout pattern is a result of plotting the locations of all the disks that comprise the nuclear cloud. The finer the mesh of disks in the cloud is made, the more accurate the pattern on the ground will be. The DELFIC program, for instance, uses 100 disks to describe the vertical distribution of the activity. Each of these disks is then further subdivided into 100 additional disks with a representative particle size describing 0.01% of the original activity of the initial disk. This means that the DELFIC code actually follows 10,000 separate disks. This mesh is considered to be fine enough to predict relatively accurate fallout patterns. However, even mainframe computers need considerable time to handle the data required for such a fine mesh. But, when only the relative amplitude across the pattern at any downwind location is required, as it is for the study of shear growth with time, only a sub set of all possible disks must be analyzed. This simplifies and speeds up the process. This simplification allows the program to run handily on even a microcomputer.

Building the Pattern

A disk tosser code, like DELFIC, does not permit snap-shot analysis of fallout along a crosswind axis. When the downwind axis is considered as a time line, as in Figure 10, then the crosswind axis becomes a time-slice of the developing fallout pattern. With the particles constrained to fixed

55

starting altitudes, the different disks, which are further defined by their 100 particle radii, fall at different velocities as determined by equation (30). This means that no two disks arrive on the ground at the same time. Therefore, the centers of the grounded disks are offset in both X and Y. This offset makes it necessary to analyze all of the disks which have fallen prior to the chosen time of analysis so that, by adding the two dimensional circular normal functions which describe the activity in the grounded disks, the correct amplitude at any ground location can be found.

A two step sorting process is used to overcome the need to analyze all of the disks mentioned above. First, Colarco's equation (31) is used to determine the approximate particle size which arrives at the arrival time of interest. Second, the radii predicted by equation (31) are used as delimiters in an iterative routine which processes the 100 equal activity radii through equation (30) with altitude parameters established by the initial stabilized cloud top and cloud bottom. This effectively establishes crude starting altitudes for the full range of particles that arrive close to the desired time of arrival. Table IX is an example of this sorting process where cloud top was set at 18,000 m and cloud bottom was set at 1000 m. The vertical increment is 1000 m.

The results of the initial sort are, understandably, only crude approximations. The process of sorting is continued to whatever degree of accuracy is desired. As the sort is

56

Table IX

Initial Sort of Radii to Determine Starting Altitude
Δz = 1000 m : Cloud top = 18000 m : Cloud bottom = 1000 m
Input arrival time for equation (31) = 3 hrs

Radius (μm)	t_a (hrs)	Altitude (m)	Radius (μm)	t_a (hrs)	Altitude (m)
1917	.1956835	18000	71.4	3.128213	12000
1064	.2801108	18000	68.4	3.111329	11000
782	.3478209	18000	65.5	3.076789	10000
629	.4105415	18000	62.7	3.020838	9000
529	.4720622	18000	60.1	3.2011	9000
457	.5341228	18000	57.5	3.114077	8000
403	.5964031	18000	55.1	3.304502	8000
361	.6589445	18000	52.9	3.163483	7000
326	.7246893	18000	50.7	3.368404	7000
297	.7922911	18000	48.6	3.190648	6000
272	.863637	18000	46.6	3.419007	6000
251	.9360802	18000	44.7	3.183808	5000
232	1.014603	18000	42.8	3.421722	5000
216	1.09313	18000	41.1	3.090501	4000
202	1.173736	18000	39.4	3.311883	4000
189	1.261139	18000	37.7	3.558912	4000
177	1.355295	18000	36.2	3.083957	3000
167	1.446057	18000	34.7	3.305018	3000
157	1.550671	18000	33.2	3.55466	3000
148	1.659398	18000	31.8	3.818962	3000
140	1.770279	18000	30.5	3.112994	2000
133	1.880645	18000	29.2	3.352316	2000
126	2.006053	18000	28	3.603631	2000
119	2.149685	18000	26.8	3.889906	2000
113	2.290389	18000	25.6	4.218101	2000
108	2.422538	18000	24.5	3.079243	1000
103	2.570773	18000	23.5	3.319904	1000
98.4	2.723914	18000	22.4	3.623523	1000
93.8	2.895769	18000	21.4	3.941959	1000
89.5	3.076839	18000	20.5	4.270033	1000
85.5	3.017588	16000	19.5	4.690053	1000
81.7	3.06394	15000	18.7	5.076425	1000
78.1	3.09858	14000	17.8	5.575694	1000
74.7	3.119044	13000	17	3.081959	4

note: The 17 μm particle is included to show that,
in fact, smaller particles require less than
the cut-off altitude in order to have an
arrival time near 3 hours.

continued, those radii which can not have a starting altitude within the cloud parameters and still achieve the arrival time desired, are rejected. The initial sort is quickly reduced to a group of radii which have the same arrival time. Once the final sort is accomplished, the starting altitude is used with the initial distribution data from equations (11) and (12) along with the standard formula for a gaussian distribution to determine the exact activity of the disk represented by the particular radius at that altitude. Since the total activity of any one of the 100 radii is 0.01% of the total cloud activity, the activity present in one of the disks determined by this method must be the amplitude of the gaussian at that altitude. Table X shows the results of the final sort using an altitude increment of 1.0 m. This is representative of the data that is used for the remainder of this study.

Table X Final Sort of Radii for t_a=3hr:Determination of Activity-A_0^i							
Group	Radius (μm)	Altitude (m)	Activity (Ci)	Group	Radius (μm)	Altitude (m)	Activity (Ci)
1	89.5	18323	1.96E-6	8	65.5	10664	5.17E-4
2	85.5	16863	2.41E-5	9	62.7	9914	3.27E-4
3	81.7	15553	1.28E-4	10	60.1	9244	1.87E-4
4	78.1	14373	3.60E-4	11	57.5	8614	9.66E-5
5	74.7	13313	6.24E-4	12	55.1	8044	4.78E-5
6	71.4	12323	7.55E-4	13	52.9	7534	2.33E-5
7	68.4	11464	6.92E-4	14	50.7	7023	1.05E-5

The true benefit of this sorting lies in the fact that because the disks are not allowed to spread in the X direction

due to any X shear, and therefore the radius of the grounded disks remains the same as at stabilization height, the use of a non-zero, positive X-direction effective wind guarantees that, with a time increment of 1 hour between points of analysis, there can be no overlap of the disks in the X direction. This ensures the ability to analyze the crosswind spread, at any time t, without concern that portions of the disks that landed at t-1 are overlapping the disks at time t.

Additionally, as the time of arrival increases to 24 hours, the quantity of disks arriving is reduced. This is a natural result of the initial cloud parameters which showed that only the very small particles would stabilize at the top of the cloud. The larger particles have fallen out before 24 hours passes. This leaves fewer and fewer particles airborn as time progresses. An example of this reduction is demonstrated, as shown in Table XI, in the data for disks arriving at 24 hours.

Table XI
Final Sort of Radii for $t_a=24$hr:Determination of Activity-A_0^i

Group	Radius (μm)	Altitude (m)	Activity (Ci)	Group	Radius (μm)	Altitude (m)	Activity (Ci)
1	23.5	17034	4.00E-4	5	19.5	11394	1.33E-3
2	22.4	15374	1.04E-4	6	18.7	10394	8.99E-4
3	21.4	13944	1.58E-3	7	17.8	9344	4.91E-4
4	20.5	12704	1.68E-3	8	17	8464	2.54E-4

When the particles in the sorted groups are operated on by the transport model, they form a line of points in the crosswind direction parallel to the Y axis. The single particle

which defines the center of each of the disks lands at the determined point. The point is expanded in the X and Y directions by application of the two gaussian distributions which originally defined the disk at stabilization. (See Figure 13)

The lack of an X shear leaves the gaussian distribution defining the downwind spread of activity in each disk unchanged. The activity in the disk would normally have to be defined by a circular normal probability distribution, where the amplitude at any point is (19:936),

$$P(x,y)=[1/(2\pi\sigma_y\sigma_x)] \; e^{-1/2\{[(x-m_x)/\sigma_x]^2+[(y-m_y)/\sigma_y]^2\}} \tag{32}$$

but, with $\sigma_y=\sigma_x$ at stabilization, and the median of the downwind distribution constrained to be on the crosswind axis by the sorting process, where $m_x=x$, equation (32) reduces to

$$P(y)=[1/(2\pi\sigma_0^2)] \; e^{-1/2[(y-m_y)/\sigma_0]^2} \tag{33}$$

where

y is any point along the radius of the disk (km),

m_y is the point calculated by the transport model (km).

Also, with the distribution in X unchanged, the peak of the distribution must have a relative amplitude of 0.3989 (20: 584). This allows further reduction of equation (33) to a single distribution in the Y direction. The amplitude of any point
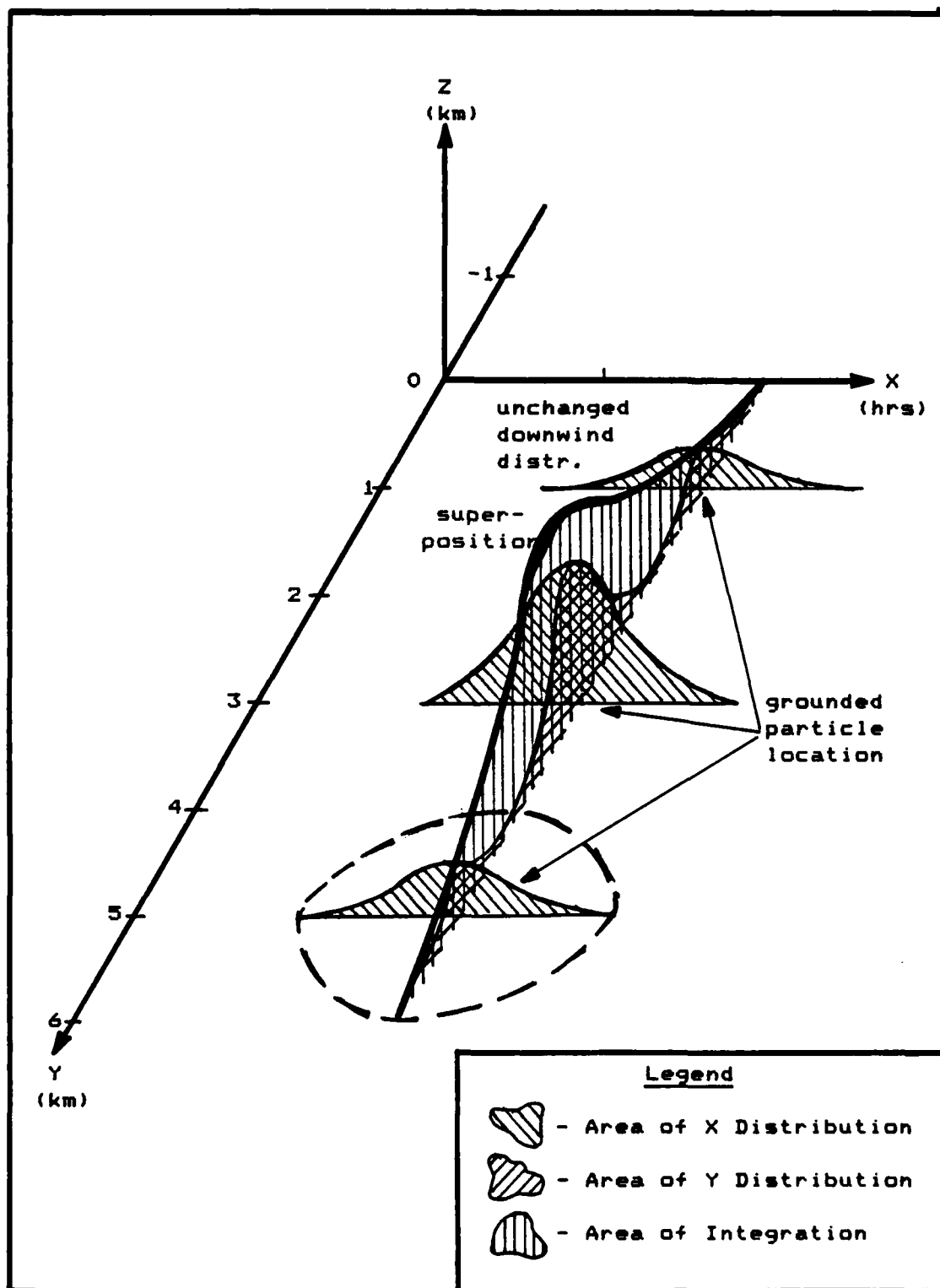
60

Figure 13. Crosswind Pattern Model

along the distribution can now be determined by integrating all the disks along the crosswind axis, or,

$$Act(y) = \int_{-\infty}^{+\infty} \frac{0.39 A_0^i}{\sqrt{2\pi\sigma_0}} e^{-1/2[(y-m_y)/\sigma_0]^2} dy \quad (Ci) \quad (34)$$

where A_0^i is the initial activity of the disk determined by the sorting process.

When equation (34) is analyzed from minus infinity to plus infinity, it produces mathematically complete solutions. However, realistically, the pattern does not extend to infinity. The model uses a limit of $3\sigma_0$, instead of infinity. Since this study does not consider an actual pattern, the $3\sigma_0$ limit is used simply to speed computation and assist in graphical presentation. The implementation of these limits is demonstrated on a specific example.

During the numerical integration along the crosswind axis, the model invokes some fundamental identities of the gaussian distribution. The gaussian distribution is centered about the median, μ , with 68% of the total area under the curve between $\mu - \sigma$ and $\mu + \sigma$. This leaves 16% of the total area in the two "tails" (1:929). Since each of the disks' activity is distributed in a gaussian manner, superpositioning the distributions of all the disks also forms a gaussian distribution. Every point of activity determined by equation (34) is the amplitude of the superpositioned gaussian distribution. As the activity is determined along the axis, the

62

amplitude is used in a trapezoidal integration routine to determine the area under the superposition. Those points along the crosswind axis which, after being analyzed to determine the amplitude of the activity there, sweep out an area of the superposition equal to 16%, 50%, and 84% are, respectively, the upwind σ_{yu}, the median (or hotline), and the downwind σ_{yd}. (Here, upwind and downwind refer to the crosswind direction.) Just as there was a difference in σ_{zT} and σ_{zB} in the model of the stabilized cloud (refer to Figure 6), a difference in σ_{yu} and σ_{yd} is expected.

As with the two previous portions of the complete model, some examples of the crosswind model in operation are examined next. Figures 14, 15, and 16 show the superpositioned gaussian distribution for arrival times of 3, 12, and 24 hours. The shear value is 0.2 km/hr/200 m. The left limit of activity is obtained by subtracting $3\sigma_0$ from the grounded location of the upwind-most particle in the 3 hour arrival group. The right limit of activity is obtained by adding the same to the downwind-most particle in the 24 hour arrival group. (From equation (5), a 1 Mt yield results in $\sigma_0 = 2.9376$.) The amplitudes are uniformly increased to permit viewing. The perspective is from a point along the Y axis. Ground zero is indicated by "GZ." Finally, because only the relative amplitude is of concern in this process, no amplitude scales are included.

The data used for these plots is presented in Appendix B. The final output of the three phased model is composed of
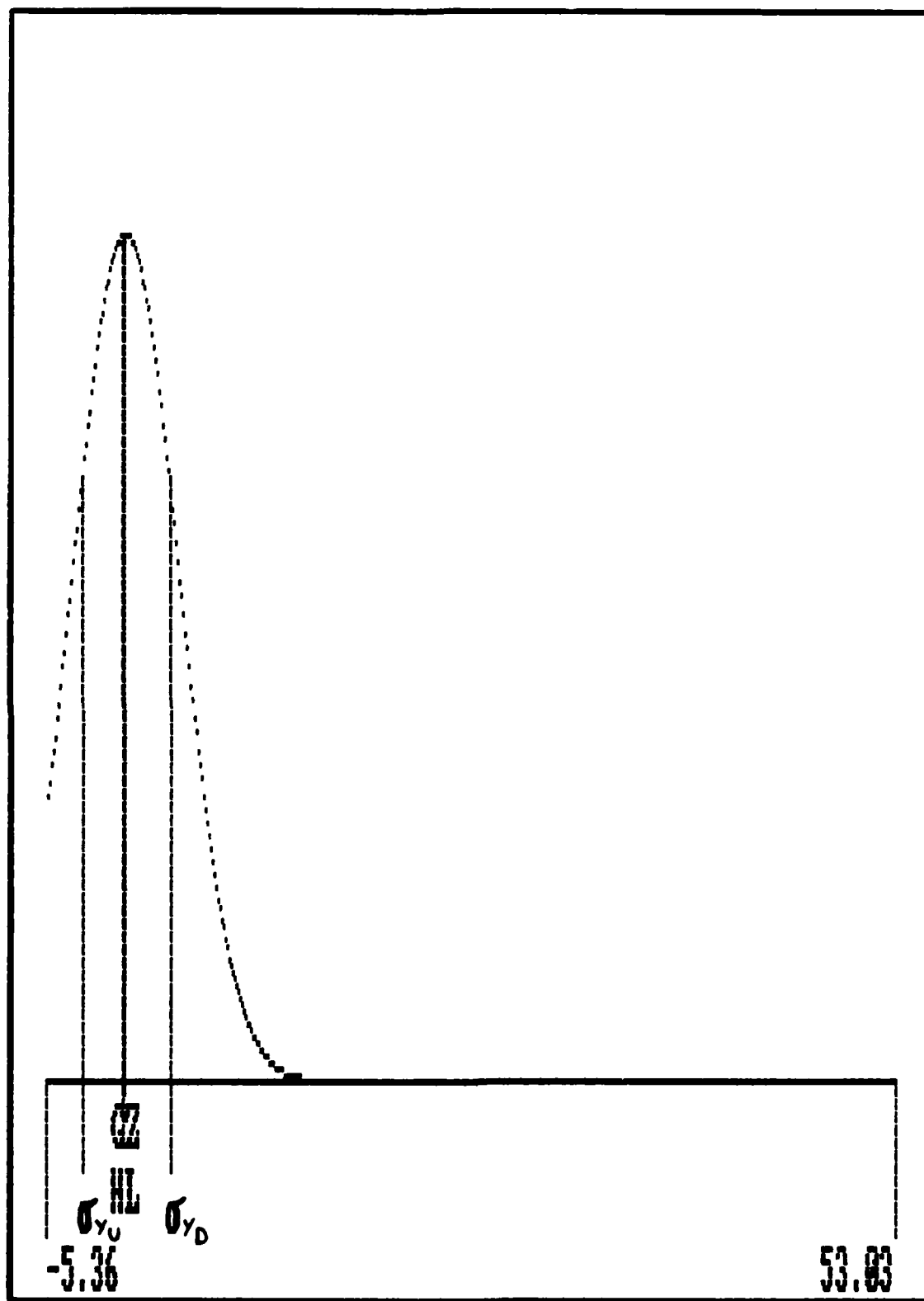
63

Figure 14. Plot of Crosswind Distribution: t_a=3hr

64
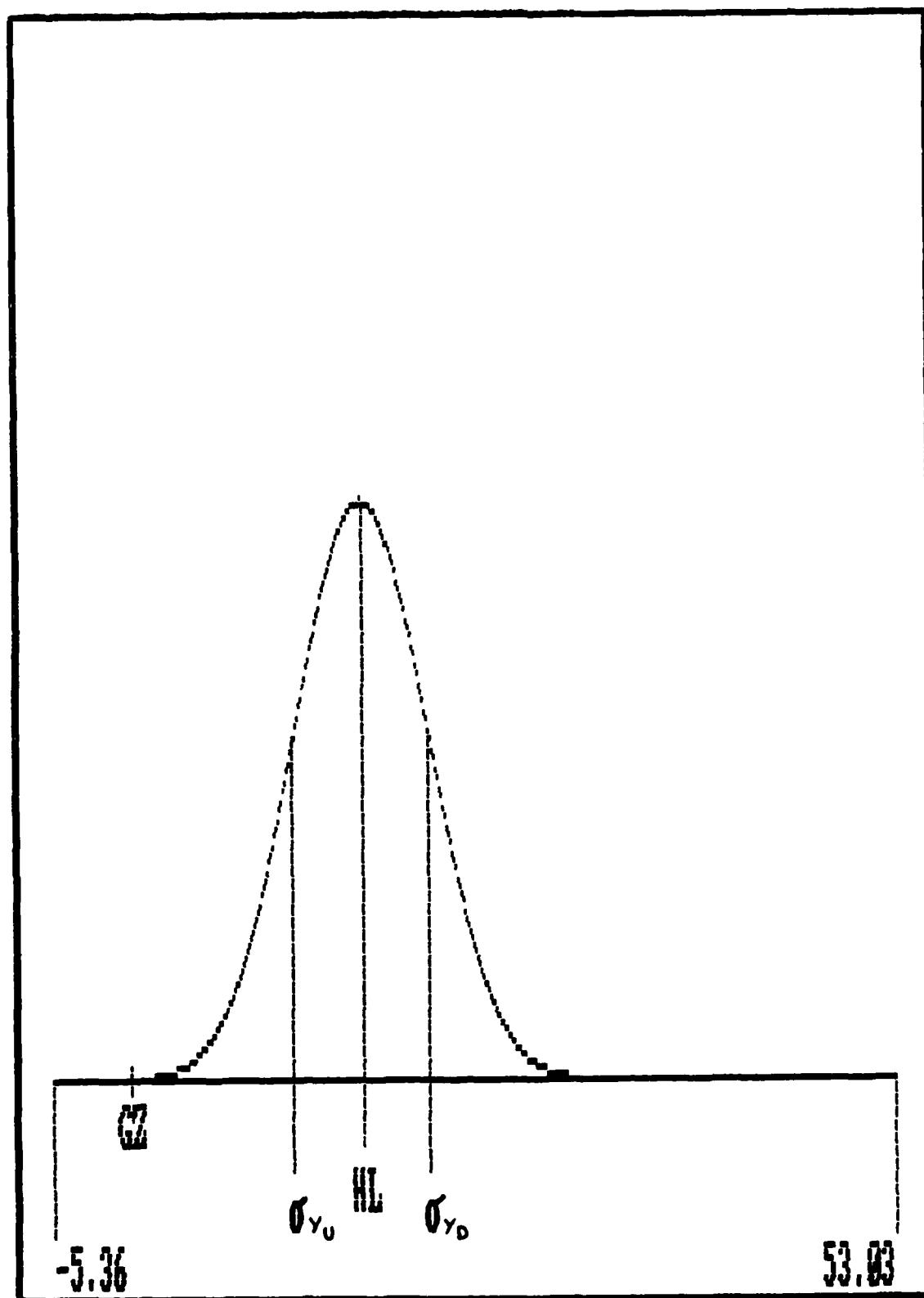
Figure 15. Plot of Crosswind Distribution: t_a=12hr
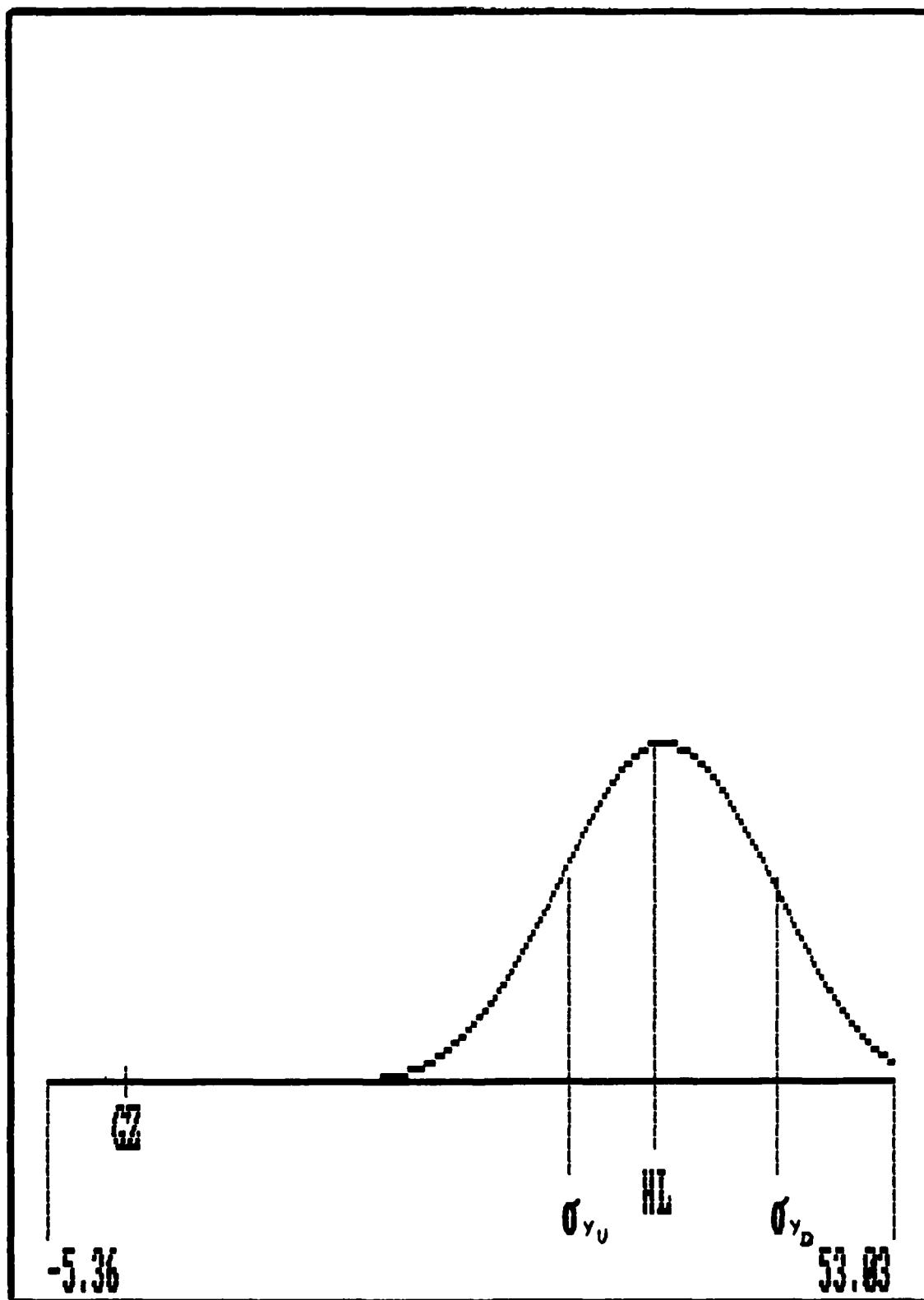
Figure 16. Plot of Crosswind Distribution: $t_a = 24hr$

66

all the σ_y calculated by the crosswind patterns. It is, therefore, particularly significant to understand exactly what values the crosswind model determines. A clear interpretation leads to enhanced understanding of the final output.

Interpreting the Pattern

Four significant items are demonstrated by the crosswind activity plots that affect subsequent analysis.

Unlike the traditional fallout patterns that have closed shapes, the analysis based on the mass of grounded fallout does not appear to have a closed configuration. This is a logical consequence of the cloud and transport models. The cloud model would, if not arbitrarily constrained to some cloud top limit, continue to predict smaller and smaller particles at higher and higher altitudes. As is evident by Tables V and VI, the smaller particles will be carried further than the larger particles. In practice, when the dose rate is calculated, the particles landing at late times carry very little of the initial activity. The fallout patterns that predict dose rate contours thus show negligible dose rates for late times. This model, on the other hand, continues to carry these particles to ever greater distances. This phenomenon is clearly visible in the three activity plots shown in Figures 14, 15, and 16. The activity pattern gets increasingly wider with time. Because the total activity is conserved, as the width increases the amplitude must decrease. This preserves the area of each of the activity plots

67

at unity. However, since the quantity of disks landing at later times is reduced from that landing at earlier times, the activity plot for 24 hours can be seen to be less smooth towards the right limit of the pattern. This is an inherent shortcoming of the discrete mesh used by all disk tossing codes. It causes fluctuations in the determination of activity by the integration routine for times greater than 20 hours which must be considered when analyzing the final output.

The difference in σ_{zT} and σ_{zB} is expected to manifest itself in the grounded activity plots. An unexpected result of analyzing the two grounded σ_y is the reversal of the difference in magnitude. At early times σ_{yu} is greater than σ_{yd}. This difference decreases to the 7 hour mark where they are nearly equal. σ_{yd} then grows larger than σ_{yu}. (See Table XII, below.) This is a result of the particle activity distribution. The heavier particles at the bottom of the cloud fall out in the early activity plots, thus creating more activity to the left, or upwind, side of the median of the distribution. At later times ($t_a > 7$ hours) the increasingly smaller particles are carried proportionately further from the hotline on the downwind side. This stretches the pattern out in the downwind direction and increases the downwind σ_{yd} correspondingly. A different particle-activity distribution would exhibit a different spread of σ_y.

Despite the aberrations in the activity plots for times greater than 20 hours, the shape of the activity plots verifies

68

the initial assumption that the crosswind activity is distributed in a gaussian manner. Although this is self evident, had a different curve emerged after superpositioning, subsequent analysis would have had to have been modified along with the initial assumption.

		Table XII			
		Differences in σ_{yu} and σ_{yd} (Calculated for a shear of 0.2 km/hr-km)			
t_a (hrs)	Left Particle Location (km)	Right Particle Location (km)	σ_{yu} (km)	σ_{yd} (km)	Difference (km)
3	3.4567	5.5321	2.9785	2.9065	-.072
4	4.6492	7.1939	2.9973	2.9263	-.071
5	5.3922	9.2362	3.0375	2.9805	-.057
6	6.4844	10.8744	3.1410	3.113	-.028
7	7.2469	13.0132	3.258	3.2594	.001
8	8.3434	14.4568	3.33	3.344	.014
9	9.7367	16.4707	3.429	3.454	.025
10	11.4742	18.0313	3.529	3.560	.031
11	12.0857	20.4215	3.6495	3.7085	.059
12	12.8071	22.1979	3.7710	3.844	.073
13	13.7391	23.9945	3.9059	3.9719	.066
14	14.7787	24.8878	4.0005	4.0765	.076
15	15.9114	26.9937	4.1625	4.2445	.082
16	17.3221	29.0556	4.3064	4.4024	.096
17	18.7959	31.1628	4.4190	4.526	.107
18	18.035	32.0484	4.6440	4.763	.119
19	19.8703	34.5593	4.8150	4.953	.138
20	22.0551	36.8599	4.9680	5.113	.145
21	21.2974	37.8385	5.2694	5.4284	.159
22	23.6951	40.5052	5.3820	5.554	.172
23	22.8833	41.491	5.6024	5.7944	.192
24	25.369	44.2221	5.6565	5.8715	.215

Finally, the transport model deposits some particles for the early times very close to the effective downwind axis. This follows from the assumption that torroidal growth can be ignored for this analysis. Without torroidal growth in the first three

69

hours, there are no mechanisms operating on σ_0 to cause the cloud, and therefore the disks, to expand during transport. Since the model for crosswind activity establishes an upwind limit of 3 σ_0, the activity plots for the early times spread activity upwind of the effective downwind axis. This causes the model to predict the hotline to move to the origin at $t_a = 0$. This has to be true and, therefore, verifies that the model is correctly modeling the actual process.

This completes the three phased model for the prediction of lateral growth. Before analyzing the model's complete output some "benchmark" plots of lateral growth are quickly discussed so that a comparison of the this model's output with the established expressions can be accomplished.

VIII. Comparisons with WSEG, Norment and Bridgman

WSEG-10 Growth Predictions

WSEG-10 can very quickly be plotted for three values of shear using the definition of crosswind shear from equation (2). The three shear values are 0.2, 0.6, and 1.0 km/hr-km.
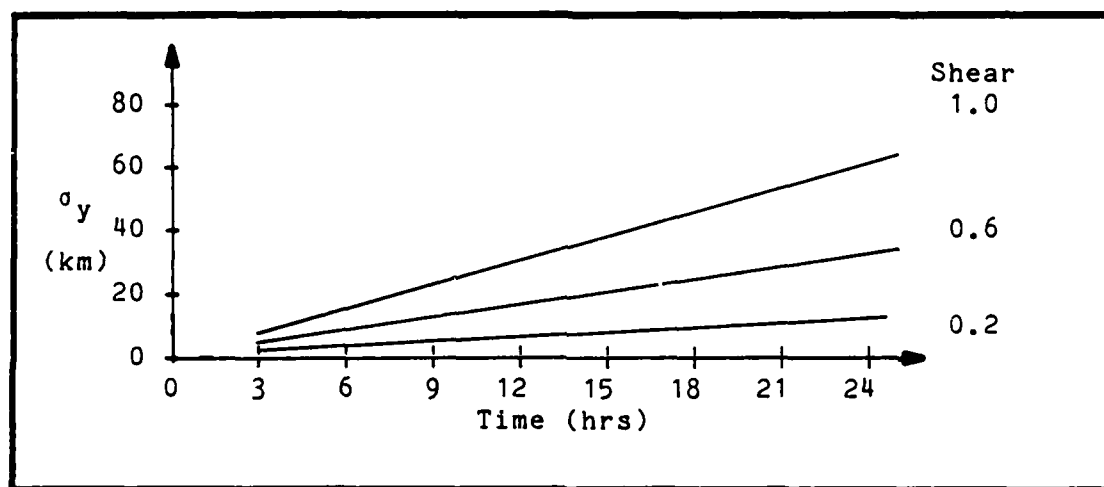
Figure 17. WSEG-10 Lateral Growth Predictions

Norment Growth Predictions

Similarly, Norment's predictions can be plotted for the same three shear values using equation (4). z_T and z_B are computed by two empirical formulas shown by Norment (6:19) as,

$$z_B = aW^b \qquad \text{(m)} \qquad\qquad (35)$$

and

$$z_T = cW^d \qquad \text{(m)} \qquad\qquad (36)$$

where

$$a = 2661 \ : \ b = 0.2198$$

$$c = 6474 \ : \ d = 0.1650$$

$$W = 1000 \ kt.$$

These equations produce $(z_T - z_B) = 8091.9$ m.
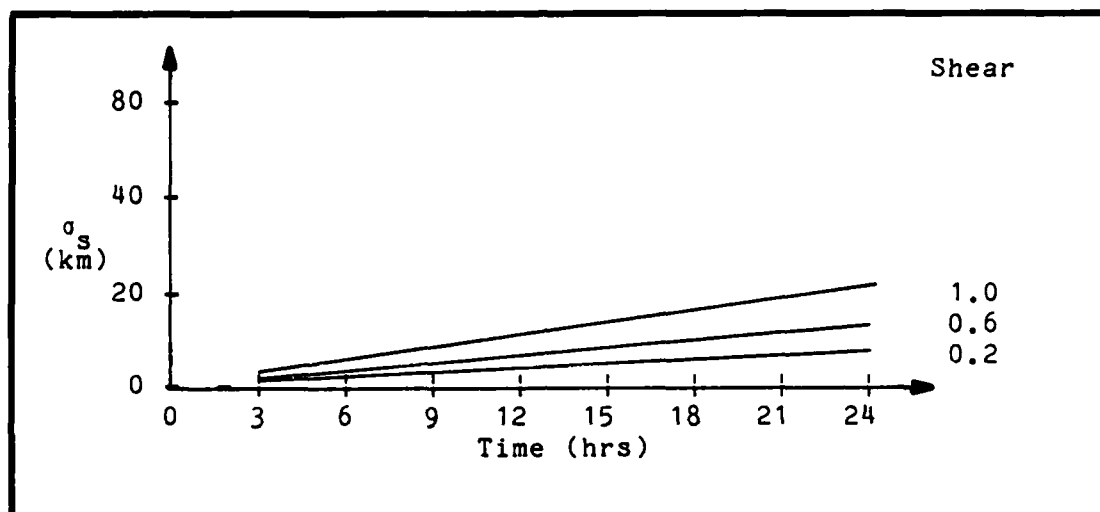
Figure 18. Norment Lateral Growth Predictions

Bridgman. C. J. Bridgman, during the process of advising the conduct of this research effort, derived a third equation for the growth of σ_s. His unpublished derivation is introduced here in order to show the origin of the final equation that is used as a "benchmark" for the results of the model explained in this study.

Bridgman's derivation begins with the knowledge that the difference between the grounded location of a particle originating at h_c and the grounded location of a particle originating at $h_c + \sigma_z$ is σ_y. Then, looking at the particle which

72

started at h_c,

$$Y_1 = \int_0^t v_z dt \tag{37}$$

Substituting $v_z = S_y[z_0 - z(t)]$ into equation (37) and making a change of integration limits using $dt = -(dz/v_z)$ yields,

$$Y_1 = \int_z^0 S_y(z_0 - z)(-dz/v_z) \tag{38}$$

He then makes the assumption that the change in the fall velocity over the range of the particle's fall is small compared to the initial velocity. This allows replacement of the v_z in equation (38) with an average fall velocity, $\langle v_z \rangle$. Now, integrating, and combining terms yields,

$$Y_1 = (S_y z_0^2)/(2\langle v_z \rangle) \tag{39}$$

Letting $\langle v_z \rangle = z_0/t$ in equation (39) then produces

$$Y_1 = S_y t z_0/2 \tag{40}$$

Repeating this process for the particle originating at $h_c + \sigma_z$ leads to,

$$Y_2 = S_y t(z_0 + \sigma_z)/2 \tag{41}$$

Clearly, when $Y_2 - Y_1 = \sigma_y$, equation (40) subtracted from equation (41) produces another expression for the growth of lateral dispersion defined as,

$$\sigma_s = S_y t \sigma_z/2 \qquad (km) \tag{42}$$

73

where

S_y is the crosswind shear (as before),

t is equivalent to t_a .

Equation (42) is very similar to the shear term in WSEG (equation 2) except for a factor of one half.
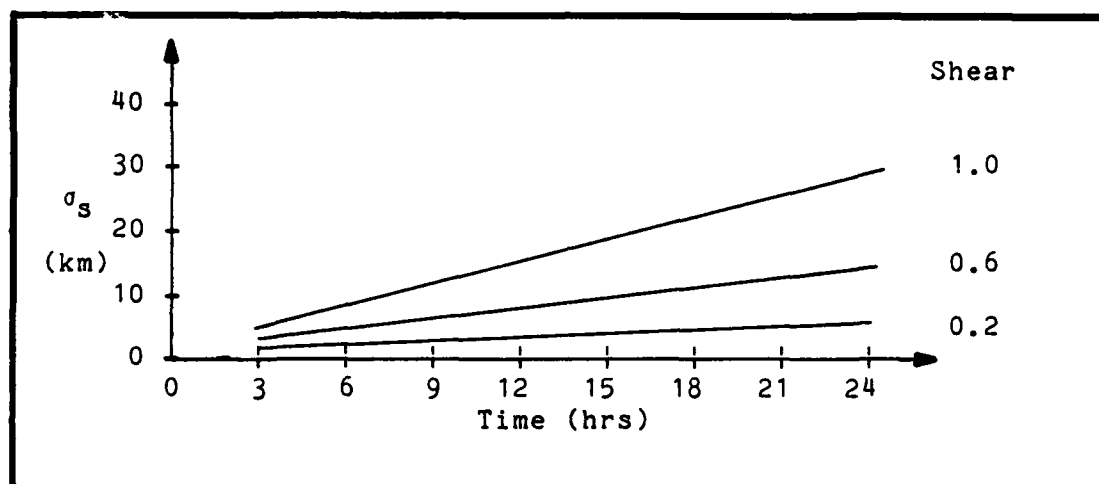
Figure 19. Bridgman Lateral Growth Predictions

These three plots are exactly what one would predict by simply comparing the three expressions (WSEG-10, Norment, and Bridgman). They are all linear and they differ only in the magnitude of the gradient. It should be obvious that the degree of fit between the model and any of these three will also be directly proportional to the shear value chosen to make the comparison with. Consequently, only one value of shear (.2 km/km-hr) will be used for the subsequent final comparison between the model and the three expressions for lateral growth.

IX. Results and Conclusions

Results

The simplest and quickest method of comparing the model's output with the expressions presented by WSEG-10, Norment, and Bridgman is to plot all four simultaneously for a particular value of shear. Shown in Figure 20 is such a plot where the shear value is 0.2 km/hr-km.

The WSEG-10, Bridgman, and Norment expressions are plotted exactly as they are shown in Figures 16, 17, and 18. As a reference point, the value of σ_s at 24 hours is included on the right edge. Again, these three expressions plot as straight lines.

The results of the model are also plotted. The shear contribution is extracted from the data developed by the model for the total lateral spread (as shown in Table XII) in the same manner that was applied to WSEG-10's equation (equations 1 to 3).

On this scale, it appears that the model predicts a σ_s which asymptotically approaches the plot of σ_s predicted by Bridgman's equation. Although the plot of WSEG-10's expression intersects the model's plot between 3 and 6 hours, it obviously diverges rapidly from the model's prediction at later times. The predicted growth from the WSEG equation is sufficiently different from the results predicted by the model that the WSEG equation will be disregarded from this point on. Both Norment

75
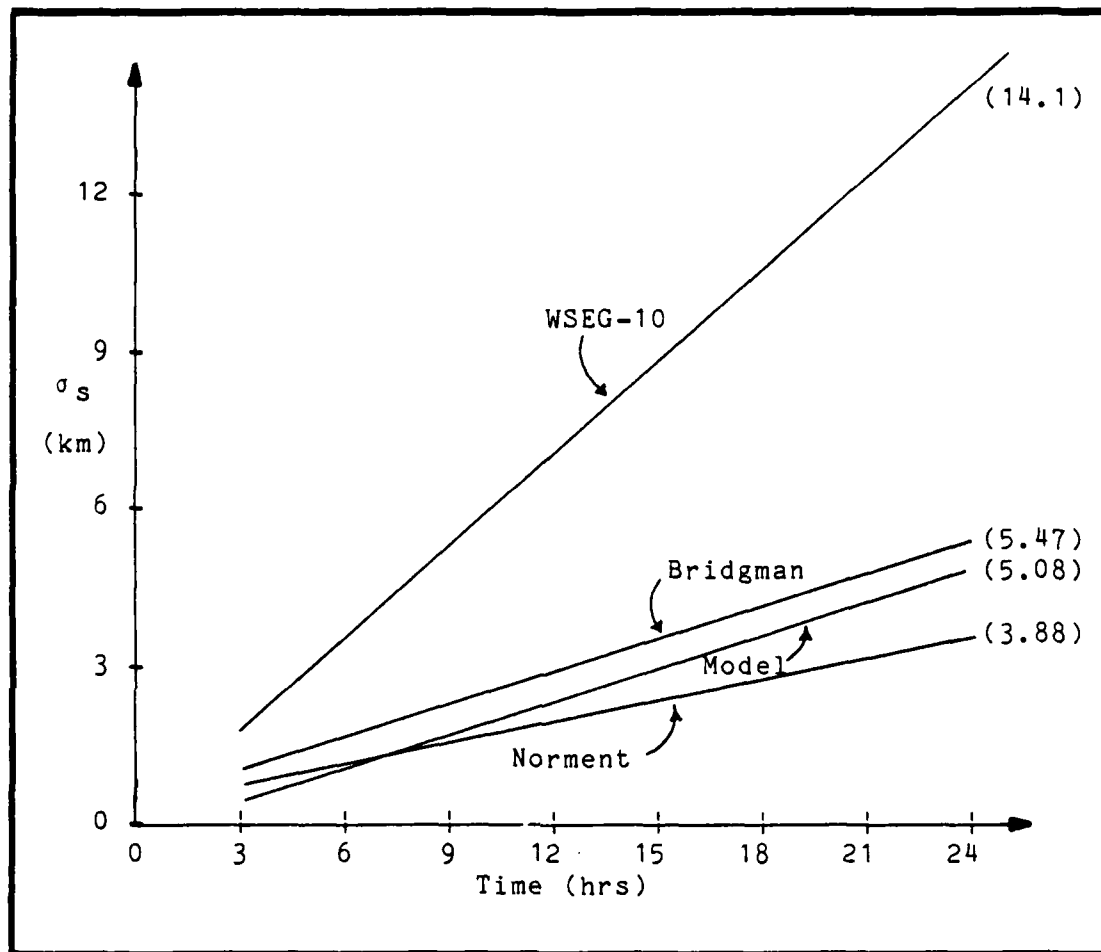
Figure 20. Four Separate Predictions of σ_s

and Bridgman's equations will be examined on a larger scale before discarding one or the other.

Figure 21 shows the results from the Bridgman and Norment equations and the model's results. Shear remains at 0.2 km/hr-km. Additionally, both σ_{yu} and σ_{yd} (from Table XII) are averaged to form a single σ_y for the model. Averaging the two σ_y from the model causes the asymptotic plot of Figure 20 to become essentially a straight line parallel to the Bridgman plot for this time domain. Norment's equation produces a line that

76
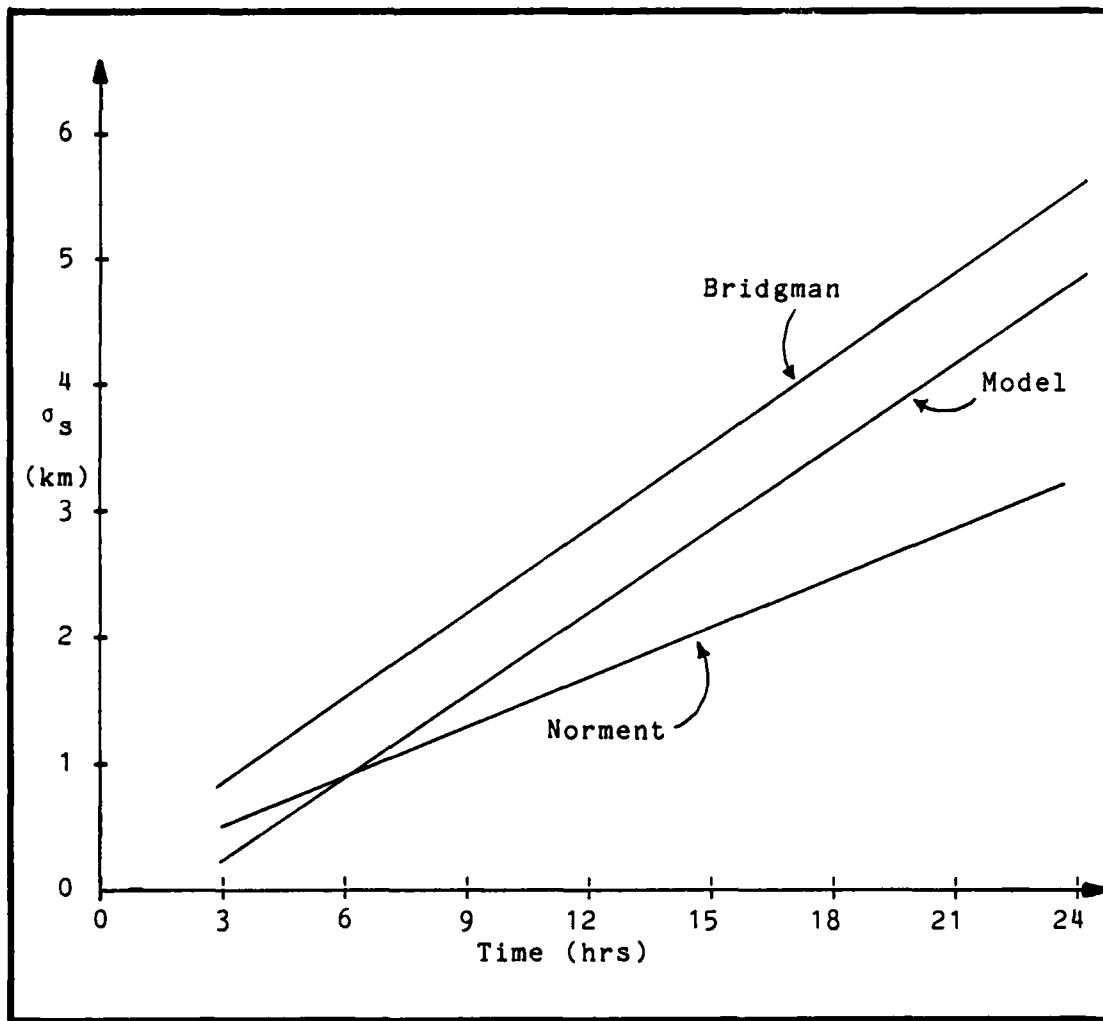
Figure 21. Three Separate Predictions of σ_s

diverges from the model as did the WSEG-10 plot. However, where
the WSEG-10 equation predicts ever larger σ_s than the model,
Norment's equation predicts the opposite.

The process of elimination leaves only one equation,
Bridgman's, that approximates both the slope and the magnitude
of the results of the model.

To insure that this correlation holds for more than this
one value of shear and is not a random occurrence, two other

77

shear values are examined. All other parameters are the same as for the 0.2 km/km-hr case just examined. Figure 22 displays the calculated values for both Bridgman's and the model's predictions for shear values of 0.6 and 1.0 km/km-hr.

Conclusions

This study has examined the processes that cause fallout particles to be spread in a crosswind direction. An improved model of the initial stabilized cloud and a discrete altitude dependent fall model have allowed these processes to be accurately modeled. From the widths of the crosswind patterns as determined by the model, it is clear that none of the initial three equations accurately predict the crosswind spread. Dr. Bridgman's equation is the best analytical method for predicting the kinds of σ_s that the model found. As is evident in Figures 21 and 22, it is valid for the range of shear values currently considered to exist in the lower atmosphere.

The model's disadvantages are the computation time and the unevenness of the product due to the discrete mesh of the particle distribution with altitude. The disadvantage of Bridgman's equation is that an average fall time must be assumed. This assumption leads to predictions of σ_s that are more accurate than the other equations analyzed but still not as accurate as the model. However, the close agreement between the new equation formulated by Bridgman and the results of the model, make an excellent case for using Bridgman's equation for predicting the lateral growth of fallout.

78
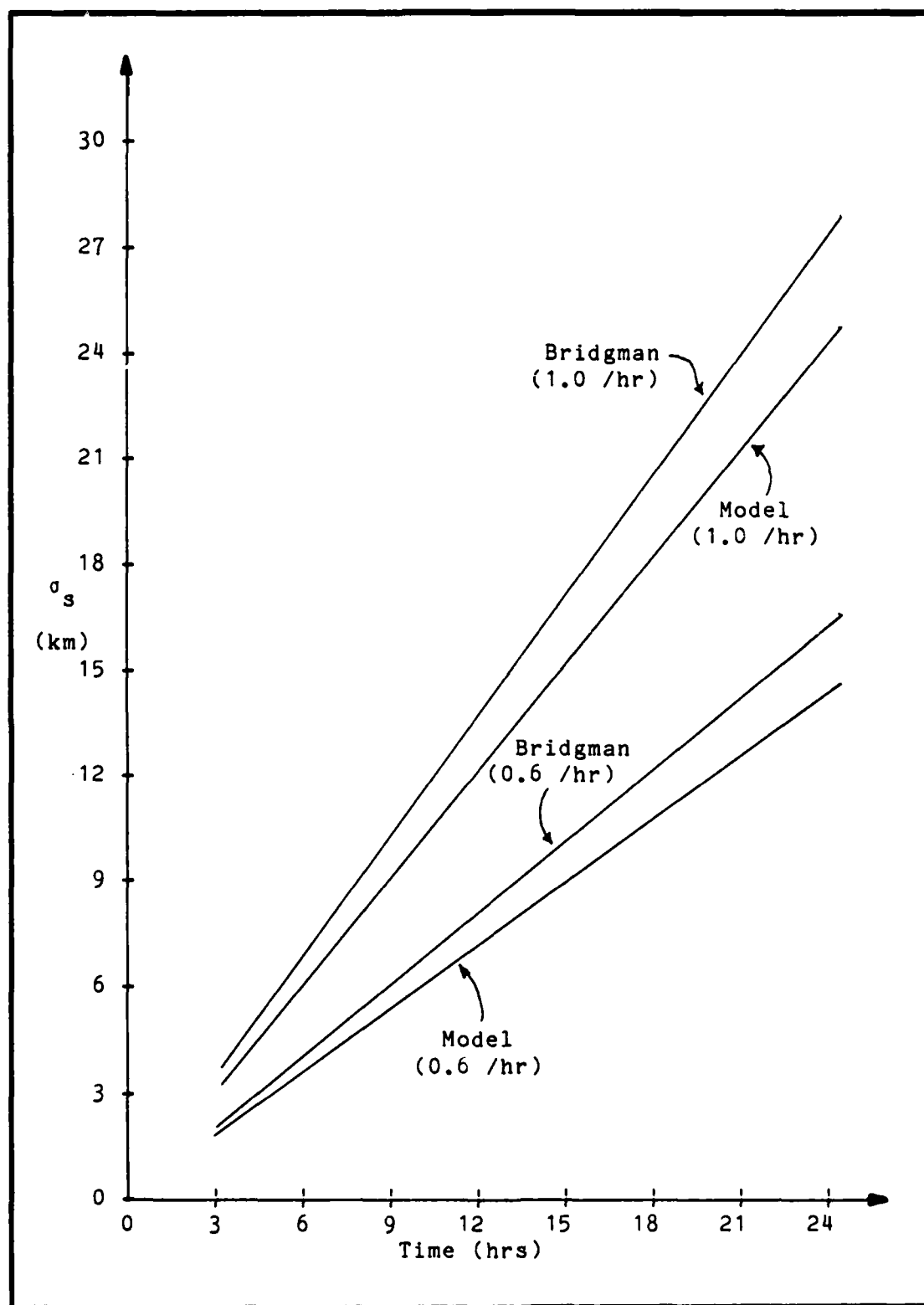
Figure 22. σ_s Comparison for Shears of 0.6 and 1.0 km/km-hr

79

X. Recommendations

There are four recommendations for the further development of this topic.

First, the development of a comprehensive model of torroidal circulation could be undertaken. This would allow a more detailed analysis of the period of cloud growth at very early times. It would also help to define a number of assumptions that are made, now, simply because no good model can be found.

Second, a variety of particle-activity distributions could be used to describe different initial stabilized clouds. These could then be matched with actual cloud data with the goal *of determining the most appropriate particle distribution to use* in conjunction with the model developed here.

Third, an analysis of the $\langle v_z \rangle$ term in Bridgman's derivation would allow more detailed study of the validity of his assumption. Furthermore, it could lead to an expression for lateral growth that is a function of weapon yield.

Lastly, a study of the multi-burstscenario could be attempted. Whereas the single burst can be modeled with a gaussian distribution, the multiple burst cloud and fallout pattern would require a different distribution.

Appendix A

DELFIC 100 Equal-Activity Group Stabilization Data

Group	Radius (μm)	h_c (km)	σ_z (km)
1	1917	0.0	0.206488
2	1064	0.0	0.987598
3	782	0.0	1.24583
4	629	0.836141	1.38594
5	529	2.87594	1.47751
6	457	4.34459	1.54344
7	403	5.44608	1.59289
8	361	6.3028	1.63135
9	326	7.01673	1.6634
10	297	7.60827	1.68996
11	272	8.11822	1.71285
12	251	8.54658	1.73208
13	232	8.93414	1.74948
14	216	9.2605	1.76413
15	202	9.54608	1.77695
16	189	9.81125	1.78886
17	177	10.056	1.79984
18	167	10.26	1.809
19	157	10.464	1.81816
20	148	10.6476	1.8264
21	140	10.8108	1.83373
22	133	10.9535	1.84014
23	126	11.0963	1.84655
24	119	11.2391	1.85296
25	113	11.3615	1.85845
26	108	11.4635	1.86303
27	103	11.5655	1.86761
28	98.4	11.6593	1.87182
29	93.8	11.7531	1.87603
30	89.5	11.8408	1.87997
31	85.5	11.9224	1.88363
32	81.7	12.0	1.88711
33	78.1	12.0734	1.89041
34	74.7	12.1427	1.89352
35	71.4	12.2101	1.89654
36	68.4	12.2712	1.89929
37	65.5	12.3304	1.90195
38	62.7	12.3875	1.90451
39	60.1	12.4405	1.90689
40	57.5	12.4936	1.90927

Group	Radius (μm)	h_c (km)	σ_z (km)
41	55.1	12.5425	1.91147
42	52.9	12.5874	1.91349
43	50.7	12.6323	1.9155
44	48.6	12.6751	1.91742
45	46.6	12.7159	1.91925
46	44.7	12.7547	1.92099
47	42.8	12.7934	1.92273
48	41.1	12.8281	1.92429
49	39.4	12.8628	1.92585
50	37.7	12.8975	1.9274
51	36.2	12.9281	1.92878
52	34.7	12.9587	1.93015
53	33.2	12.9893	1.93152
54	31.8	13.0178	1.93281
55	30.5	13.0443	1.934
56	29.2	13.0708	1.93519
57	28	13.0953	1.93629
58	26.8	13.1198	1.93739
59	25.6	13.1443	1.93848
60	24.5	13.1667	1.93949
61	23.5	13.1871	1.94041
62	22.4	13.2096	1.94141
63	21.4	13.23	1.94233
64	20.5	13.2483	1.94315
65	19.5	13.2687	1.94407
66	18.7	13.285	1.9448
67	17.8	13.3034	1.94563
68	17	13.3197	1.94636
69	16.1	13.3381	1.94718
70	15.4	13.3523	1.94782
71	14.6	13.3687	1.94856
72	13.9	13.3829	1.9492
73	13.2	13.3972	1.94984
74	12.5	13.4115	1.95048
75	11.8	13.4258	1.95112
76	11.2	13.438	1.95167
77	10.6	13.4502	1.95222
78	10	13.4625	1.95277
79	9.45	13.4737	1.95327
80	8.89	13.4851	1.95379

Group	Radius (µm)	h_c (km)	σ_z (km)
81	8.35	13.4961	1.95428
82	7.82	13.507	1.95477
83	7.32	13.5172	1.95522
84	6.83	13.5271	1.95567
85	6.35	13.5369	1.95611
86	5.89	13.5463	1.95653
87	5.45	13.5553	1.95694
88	5.02	13.5641	1.95733
89	4.6	13.5726	1.95771
90	4.19	13.581	1.95809
91	3.8	13.589	1.95845
92	3.41	13.5969	1.9588
93	3.04	13.6045	1.95914
94	2.68	13.6118	1.95947
95	2.32	13.6191	1.9598
96	1.97	13.6263	1.96012
97	1.62	13.6334	1.96044
98	1.27	13.6406	1.96076
99	.904	13.648	1.9611
100	.473	13.6568	1.96149

Appendix B

Data for Activity Distribution Plots

t_a = 3 hours:

Radius (μm)	Grounded Location (km)	Activity-$A_0{}^i$ (Ci)
85.5	3.45673	4.51982E-4
81.7	3.76633	9.59174E-4
78.1	4.0525	1.44708E-3
74.7	4.31519	1.68805E-3
71.4	4.56274	1.62146E-3
68.4	4.78215	1.35534E-3
65.5	4.99054	1.01696E-3
62.7	5.18892	6.99137E-4
60.1	5.35708	4.58880E-4
57.5	5.53205	2.86741E-4

t_a = 12 hours:

34.7	12.8071	3.66634E-4
33.2	14.3793	9.02291E-4
31.8	15.7713	1.44682E-3
30.5	17.0255	1.69530E-3
29.2	18.2353	1.56075E-3
28.0	19.307	1.19573E-3
26.8	20.3353	7.80603E-4
25.6	21.3185	4.46510E-4
24.5	22.1979	2.45446E-4

t_a = 24 hours:

23.5	25.3690	4.00393E-4
22.4	29.0203	1.03766E-3
21.4	32.2468	1.57847E-3
20.5	34.9277	1.68178E-3
19.5	37.7679	1.32815E-3
18.7	39.9412	8.99450E-4
17.8	42.2687	4.91404E-4
17.0	44.2221	2.53800E-4

Bibliography

1. Kreyszig, Erwin. _Advanced Engineering Mathematics_ (Fifth Edition). New York: John Wiley and Sons, 1983.

2. Glasstone, Samuel. and Philip J. Dolan. _The Effects of Nuclear Weapons_ (Third Edition). Washington D.C.: U.S. Government Printing Office, 1977.

3. Hanifen, Dan W. _Documentation and Analysis of the WSEG-10 Fallout Prediction Model._ MS Thesis, School of Engineering, Air Force Institute of Technology (AU), Wright-Patterson AFB OH, March 1980 (AD A083 515).

4. Pugh, George E. _Revision of Fallout Parameters for Low-Yield Detonations._ Supplement to WSEG Research Memorandum No. 10, Weapon Systems Evaluation Group, The Pentagon, Washington D.C., 7 November 1978 (AD A061 536).

5. Pugh, George E. and Robert J. Galiano. _An Analytic Model of Close-In Deposition of Fallout for Use in Operational-Type Studies._ WSEG Research Memorandum No. 10, Weapon Systems Evaluation Group, The Pentagon, Washington D.C., 15 October 1959 (AD 26 752).

6. Norment, Hillyer G. _An Analytical Fallout Prediction Model and Code: Final Report,_ 12 March 1980--31 October 1981. Contract DNA 001-80-C-0197.Atmospheric Science Associates, Bedford, MA, 31 October 1981 (AD A130 291).

7. Breuer, D. Wallace. _The Fundamentals of Weapons Engineering Volume I_ (Second Printing). Contract F33601-81-C-0185. Air Force Institute of Technology (AU), Wright-Patterson AFB OH, February 1984.

8. Conners, Capt Stephen P. _Aircrew Dose and Engine Dust Ingestion from Nuclear Cloud Penetration._ MS Thesis, School of Engineering, Air Force Institute of Technology (AU), Wright-Patterson AFB OH, March 1985.

9. _U.S. Standard Atmosphere, 1976._ NOAA. U.S. Government Printing Office, Washington D.C.,1976.

10. Hidy, George M. _The Winds: The Origins and Behavior of Atmospheric Motion._ Princeton: D. Van Nostrand Company, Inc., 1967.

11. Kathren, Ronald L. _Radioactivity in the Environment: Sources, Distribution, and Surveillance._ New York: Harwood Academic, 1984.

12. Hopkins, Anthony T. A Two Step Method to Treat Variable Winds in Fallout Smearing Codes. MS Thesis, School of Engineering, Air Force Institute of Technology (AU), Wright-Patterson AFB OH, March 1982.

13. Panofsky, Hans A. and John A. Dutton. Atmospheric Turbulence: Models and Methods for Engineering Applications. New York: John Wiley and Sons, 1984.

14. Defense Nuclear Agency. Compilation of Local Fallout Data from Test Detonations 1945-1962, Extracted from DASA 1251, Volume I, edited by Howard A. Hawthorne. General Electric Company-TEMPO, Santa Barbara CA, 1 May 1979 (AD A079 310).

15. AFOTEC Computer Code "ARMA" Extract, LT Jeffrey R. Brown, U.S. Air Force ASD/ENSS, Wright-Patterson AFB OH, 15 October 1985.

16. Bridgman, Charles J. and Winfield S. Bigelow. "A New Fallout Prediction Model," Health Physics, 42: 205-218 (August 1982).

17. McDonald, James E. "An Aid to Computation of Terminal Fall Velocities of Spheres," Journal of Meteorology, 17: 463-465 (August 1960).

18. Colarco, Capt Richard F. A Computer Fallout Model for Operational Type Studies. MS Thesis, School of Engineering, Air Force Institute of Technology (AU), Wright-Patterson AFB OH, March 1980.

19. Zelen, Marvin. and Norman C. Severo. "Probability Functions," Handbook of Mathematical Functions With Formulas, Graphs, and Mathematical Tables, edited by Milton Abramowitz and Irene A. Stegun. Washington D.C.: U.S. Government Printing Office, 1965.

20. Selby, Samuel M., Editor. Standard Mathematical Tables, (Twenty-first Edition). Cleveland: The Chemical Rubber Co., 1973.

VITA

Captain David P. Schneider was born on ██████████████ in ██████████████████████████ As the second of five sons of a career Army officer, he spent a majority of his formative years living in foreign countries ranging from Japan to the Soviet Union to Germany. After graduating from high school in Alexandria, Virginia, he entered the United States Military Academy in 1973.

Upon commissioning in the Armor Branch, he served as a Tank Company Platoon Leader in Europe. After commanding a Tank Company in the 8th Infantry Division (Mech), CPT Schneider returned to Ft. Bliss, Texas, where he commanded C Troop, 1st Squadron of the 3rd Armored Cavalry Regiment.

In September, 1984, CPT Schneider entered the School of Engineering, Air Force Institute of Technology, Wright-Patterson Air Force Base, Ohio.

Permanent address: ███████████████████
████████████████████

87

AD-A172 769

REPORT DOCUMENTATION PAGE

1a. REPORT SECURITY CLASSIFICATION	1b. RESTRICTIVE MARKINGS
UNCLASSIFIED	

2a. SECURITY CLASSIFICATION AUTHORITY	3. DISTRIBUTION/AVAILABILITY OF REPORT
	Approved for public release;
2b. DECLASSIFICATION/DOWNGRADING SCHEDULE	Distribution unlimited.

4. PERFORMING ORGANIZATION REPORT NUMBER(S)	5. MONITORING ORGANIZATION REPORT NUMBER(S)
AFIT/GNE/PH/86M-12	

6a. NAME OF PERFORMING ORGANIZATION	6b. OFFICE SYMBOL (If applicable)	7a. NAME OF MONITORING ORGANIZATION
School of Engineering	AFIT/EN	

6c. ADDRESS (City, State and ZIP Code)	7b. ADDRESS (City, State and ZIP Code)
Air Force Institute of Technology Wright-Patterson AFB, OH 45433	

8a. NAME OF FUNDING/SPONSORING ORGANIZATION	8b. OFFICE SYMBOL (If applicable)	9. PROCUREMENT INSTRUMENT IDENTIFICATION NUMBER

8c. ADDRESS (City, State and ZIP Code)	10. SOURCE OF FUNDING NOS.			
	PROGRAM ELEMENT NO.	PROJECT NO.	TASK NO.	WORK UNIT NO.

11. TITLE (Include Security Classification)
See box 19

12. PERSONAL AUTHOR(S)
David P. Schneider, B.S., Captain, USA

13a. TYPE OF REPORT	13b. TIME COVERED	14. DATE OF REPORT (Yr., Mo., Day)	15. PAGE COUNT
Thesis (M.S.)	FROM _____ TO _____		

16. SUPPLEMENTARY NOTATION

17.	COSATI CODES		18. SUBJECT TERMS (Continue on reverse if necessary and identify by block number)
FIELD	GROUP	SUB. GR.	Nuclear Clouds, Fallout, Fallout Spreading,
01	02		Cloud Modeling, Fallout Modeling

19. ABSTRACT (Continue on reverse if necessary and identify by block number)

Title: DETERMINATION OF LATERAL SPREAD OF NUCLEAR FALLOUT PATTERNS

Thesis Chairman: Dr. Charles J. Bridgman
Professor of Nuclear Engineering
Department of Nuclear Engineering (Engineering Physics)

This report develops an improved method of determining the lateral spread of nuclear fallout. A full-physics model of pattern development based on particle mass is analyzed. A rapid, simplified method for the prediction of nuclear fallout patterns is developed for the case of a 1 Mt weapon based on empirical data from WSEG-10. This model is extended to other weapon sizes.

Approved for public release: IAW AFR 190-1.
LYNN E. WOLAVER 7 May 86
Dean for Research and Professional Development
Air Force Institute of Technology (AFSC)
Wright-Patterson AFB OH 45433

20. DISTRIBUTION/AVAILABILITY OF ABSTRACT	21. ABSTRACT SECURITY CLASSIFICATION
UNCLASSIFIED/UNLIMITED ☒ SAME AS RPT. ☐ DTIC USERS ☐	UNCLASSIFIED

22a. NAME OF RESPONSIBLE INDIVIDUAL	22b. TELEPHONE NUMBER (Include Area Code)	22c. OFFICE SYMBOL
Dr. Charles J. Bridgman	513-255-2012	AFIT/ENP

DD FORM 1473, 83 APR   EDITION OF 1 JAN 73 IS OBSOLETE.